Pten, Pi3K and PtdIns(3,4,5)P_3 dynamics modulate pulsatile actin branching in *Drosophila* retina morphogenesis

Jacob Malin[1], Christian Rosa Birriel[1] & Victor Hatini[1*]

[1]Tufts University School of Medicine, Department of Developmental, Molecular & Chemical Biology, Program in Cell, Molecular and Developmental Biology, Program in Genetics and Program in Pharmacology and Experimental Therapeutics, 150 Harrison Avenue, Boston, MA 02111, United States

*Corresponding authors: [a] Victor.Hatini@tufts.edu

ABSTRACT

Epithelial remodeling of the *Drosophila* retina depends on the generation of pulsatile contractile and protrusive forces that repeatedly contract and expand the apical contacts between the lattice cells (LCs) that form its hexagonal lattice. Phosphoinositide PI(3,4,5)P_3 (PIP_3) accumulates around tricellular adherens junctions (tAJs) when cell-cell contacts expand and dissipates when they contract, but its significance in this process is unknown. Here we found that manipulations of Pten or Pi3K that either decreased or increased PIP_3 resulted in similar phenotypes characterized by shortened contacts and a disordered lattice, indicating a requirement for dynamics and turnover of PIP_3. We further show that these phenotypes are caused by a loss of protrusive branched F-actin, the result of impaired activity of the Rac1 Rho GTPase and the WAVE regulatory complex (WRC). We additionally found that during contact expansion, Pi3K moves into tAJs where it is positioned to promote the cyclical increase of PIP_3 in a spatially and temporally precise manner. Taken together, the results show that dynamic regulation of PIP_3 by Pten and Pi3K is critical for the protrusive phase of junctional remodeling, which is essential for planar epithelial morphogenesis.

INTRODUCTION

The *Drosophila* retina serves as a model for understanding fundamental developmental biology questions such as how cells form complex organs (Cagan and Ready, 1989). The apical epithelium of the fly retina is composed of approximately 800 nearly identical ommatidia composed of stereotypically shaped and arranged cell types (Cagan, 2009; Carthew, 2007; Johnson, 2021). Pulsatile length changes of cell junctions, depending on both contractile actomyosin and protrusive branched F-actin networks, are essential to ommatidial morphogenesis (Blackie et al., 2021; Blackie et al., 2020; Chan et al., 2017; Del Signore et al., 2018; Galy et al., 2011; Hayashi and Carthew, 2004; Letizia et al., 2019; Malin et al., 2022; Zallen et al., 2002). The role of contractile actomyosin pulsing has received considerable attention in similar systems (Heer and Martin, 2017). More recently understood, however, is the active role of protrusive forces as cell contacts expand (Del Signore et al., 2018). Protrusion is regulated by the WAVE regulatory complex (WRC), which activates the Arp2/3 complex to promote F-actin branching (Rottner et al., 2021). Inhibition of either F-actin branching or actomyosin contractility impairs this balance between expansion and contraction, leading to changes in cell shape and cellular arrangement that disrupt ommatidia structure (Del Signore et al., 2018). Thus, a major goal is to determine the mechanisms that cyclically activate and inactivate cytoskeletal networks that govern both protrusion and contraction.

During eye epithelial remodeling, cell-cell contacts cycle through contractile and protrusive pulses. A central player in the control of this process at the tAJs is the homophilic adhesion molecule Sidekick (Sdk) (Letizia et al., 2019; Malin et al., 2022). Sdk dynamically associates with tAJs, where it toggles between interacting with contractile and protrusive effectors. To expand junctions, Sdk binds and causes the enrichment of the WRC, which promotes the accumulation of branched F-actin and generation of protrusive force. As the contacts expand, Sdk exchanges interactions with the WRC for Polychaetoid (Pyd), the fly Zonula Occludens-1 (ZO-1) protein. Pyd then connects the junctional actomyosin networks to the tAJs, and this causes the junctions to contract. As tension rises and contacts contract, Pyd disassembles from Sdk, allowing the WRC to bind to Sdk to initiate the next expansion cycle.

While we know that Sdk recruits the WRC and may activate it to some extent, it is likely that additional coincident signals further activate the WRC to generate protrusion. We previously discovered that the phosphoinositide phosphatidylinositol (3,4,5)-trisphosphate (PIP_3) accumulates preferentially at tAJs of expanding LC-LC contacts (Del Signore et al., 2018). *In vitro,* PIP_3 synergizes with other coincidental signals to stimulate WRC-dependent F-actin branching, raising the possibility that it could be involved in the process of contact expansion (Chen et al., 2017; Hume et al.; Koronakis et al., 2011; Mendoza, 2013; Mendoza et al., 2011; Schaks et al., 2018). In this context, Rac1 is a major protein that controls the allosteric activation of the WRC, and Rac1 function can be regulated by PIP_3 through intermediary Rac GTPase exchange factors (Cantley, 2002).

Levels of PIP_3 are regulated by two enzymes, the phosphatase and tensin homolog (Pten) and the class 1A phosphoinositide 3-kinase (Pi3K), that respectively decrease and increase its levels through dephosphorylation and phosphorylation, converting it to and from phosphatidylinositol (4,5)-bisphosphate (PIP_2) (Auger et al., 1989; Li et al., 1997; Traynor-Kaplan et al., 1988; Whitman et al., 1988). Pten and Pi3K are among the most studied proteins in biology and have been implicated in processes such as cell growth, metabolism, and survival, and as drivers of different cancers (Gao et al., 2000; Goberdhan et al., 1999; Huang et al., 1999; Oldham et al., 2002). In these processes, they have multiple known effectors (Chalhoub and Baker, 2009). For example, in addition to its lipid phosphatase activity relevant to PIP_3, Pten has known protein phosphatase activity capable of regulating multiple proteins (Qi et al., 2020). Thus, it is important to carefully analyze the relationship between these actors and their mechanism of action. While it has been observed that cell contacts are shortened in *pten* mutants in planar epithelial morphogenesis in *Drosophila*, the importance of Pten to protrusive forces has never been examined (Bardet et al., 2013).

In the regulation of actin dynamics, Pten, Pi3K and PIP_3 often exhibit highly specific subcellular distribution within cells. For example, in motile cells, high levels of Pi3K and PIP_3 promote protrusion at the leading edge of the lamellipodium, while high levels of Pten and PIP_2 promote contraction at the rear and sides (Funamoto et al., 2002). Likewise, in certain epithelia, Pten is essential for apical-basal polarity, associating with a protein located at the subapical AJs (Bazooka/Par3) and producing PIP_2, which specifies an apical identity while PIP_3 specifies basolateral identity (von

Stein et al., 2005). Selective recruitment of Pi3K to the edges of newly formed AJs has also been shown in vertebrates (Kovacs et al., 2002; Perez et al., 2008; Yamada and Nelson, 2007). However, in the context of junction remodeling during planar epithelial morphogenesis, the relative localization of Pten, Pi3K and PIP_3 has never been fully elucidated and the interactions between these factors are therefore unclear.

This study addresses this open question by examining both protrusive and contractile cytoskeletal elements and probing the function of Pten, Pi3K, and Rac1 in relation to PIP_3. We show that the Pten-Pi3K enzyme pair dynamically modulates PIP_3 as well as cytoskeletal and mechanical forces that shape the epithelium, and through live imaging, reveal the subcellular organization of this system over time. We also provide evidence that PIP_3 dynamics modulate Rac1 function, that Rac1 amplifies Pi3K function, and that both PIP_3 and Rac1 activate the WRC, F-actin branching, and contact expansion. We propose that PIP_3 dynamics regulate contact-length pulsing by controlling the cytoskeletal transition from contraction to expansion.

RESULTS

pten controls epithelial remodeling of the fly retina

To examine *pten's* role in eye epithelial remodeling, we used the Eyeless-GAL4/UAS-FLP (EGUF) technique, by which the retina can be rescued from Hid-mediated apoptosis if mutant cells can create viable tissue (Stowers and Schwarz, 1999). We used this method to generate eyes that were entirely mutant for three independent *pten* mutant alleles: $pten^{3}$, $pten^{c494}$and $pten^{2L100}$ (Devergne et al., 2014; Goberdhan et al., 1999; Oldham et al., 2002). Consistent with previous reports, our data below indicate that $pten^{3}$ and $pten^{c494}$ are strong alleles while $pten^{2L100}$ is a hypomorph (Goberdhan et al., 1999; Huang et al., 1999; Oldham et al., 2002). In wild-type (WT) eyes, ommatidia form a regular hexagonal array with a small variation in the edge length of each hexagon (Fig. 1A-B, D). Scanning electron microscopy (SEM) imaging of adult eyes revealed that, in contrast to the regular shape and tessellation of ommatidia in WT eyes, a fraction of ommatidia in *pten* mutant eyes were irregularly shaped and some were fused to one another (Fig. 1B-C'). To determine the effects of *pten* loss on epithelial organization, we examined developing eyes at 36-42h after puparium

formation (APF) after cells acquired their stable shapes (Fig. 1E-G). In *pten*^{3}, *pten*^{c494} and *pten*^{2L100} mutants, ommatidia maintained their overall structure but formed quadrilaterals and pentagons in addition to hexagons (Fig. 1H). Defects in cell arrangements included the clustering of multiple mechanosensory bristles (Fig. 1I) and the clustering of LCs around bristles, resulting in the formation of cellular "rosettes", a phenotype that can arise from impaired intercalation (Fig. 1J) (Bao and Cagan, 2005; Johnson et al., 2011; Johnson et al., 2008; Letizia et al., 2019; Malin et al., 2022; Seppa et al., 2008). In addition, some 3° lattice cells failed to occupy the corners of ommatidia, while others were missing, with the remaining LC occupying both the lattice edge and corner. Another common defect was the partial or complete loss of LC-LC contacts resulting in the separation of adjacent LCs and contact between the 1° cells of adjacent ommatidia (Fig. 1K).

To determine whether *pten* affects epithelial remodeling cell-autonomously, we generated patches of genetically marked *pten*^{3} and *pten*^{2L100} mutant cells and asked whether the cellular defects were confined to the clones, adjacent to the clones, or found in both regions (Fig. 1L-N). We found that the characteristic intercalation and cellular arrangement defects were largely confined to the *pten* mutant clones indicating that *pten* acts cell-autonomously. We also found non-autonomous defects adjacent to the clones at a lower frequency. The *pten* autonomous and non-autonomous defects are consistent with a role for *pten* in controlling force dynamics and force transmission necessary for proper epithelial remodeling. Overall, the remodeling defects in *pten*^{3} and *pten*^{c494} eyes were more severe compared with *pten*^{2L100} eyes. Therefore, we used the strong *pten*^{3} allele for subsequent experiments.

pten controls fluctuations of LC-LC contact length

During lattice remodeling, the LC-LC contacts expand and contract repeatedly. These dynamics arise from the alternate generation of protrusive and contractile forces at the level of individual LC-LC contacts (Del Signore et al., 2018). When LCs prune from the lattice, their neighbors on either side rapidly reestablish contact (Fig. 2A, Movie 1). To determine whether *pten* affects these dynamics, we live imaged *pten* mutant eyes with an α-Catenin::Venus (α-Cat::Venus) protein trap to observe apical cell outlines at the level of AJs. We observed that expansion and contraction

of LC-LC contacts appeared minimal and that temporary or permanent 1°-1° contacts were formed upon cells pruning from the lattice and sometimes spontaneously (Fig. 2B, Movie 1). We then measured the length of the LC-LC contacts over time. We excluded contacts that failed to expand following contraction and those that were being lost and replaced with 1°-1° contacts. We found that in *pten* mutants, the mean length, pulse amplitude, and pulse frequency of the LC-LC contacts decreased significantly compared with WT (Fig. 2C-D, F). However, the pulse amplitude normalized to average contact length was not significantly different from WT indicating that the shortened contacts in *pten* mutants were still pulsing (Fig. 2E). These contact pulsing defects suggest that *pten* plays a role in the rebalancing of the opposing contractile and protrusive forces that contract and expand the LC-LC contacts.

pten controls protrusive and contractile dynamics of LC-LC contacts

To better understand how Pten controls cytoskeletal dynamics, we compared F-actin and MyoII dynamics between WT eyes and fully *pten* mutant eyes. We measured the length of the LC-LC contacts in time-lapse movies, along with the signal intensities of F-actin at the vertices, where it concentrates most strongly, and MyoII along the entire contacts. We labeled F-actin with the actin-binding domain of Utrophin tagged with GFP (Utr::GFP) and followed MyoII dynamics with Spaghetti Squash (Sqh), the regulatory light chain of non-muscle Myosin II, tagged with GFP (Sqh::GFP) (Fig. 3A-D, Movies 2-3). We then computed the temporal cross-correlation between the signal intensity of either F-actin or MyoII and contact length (Fig. 3E-H). In WT, protrusive F-actin accumulated during contact expansion and peaked just prior to maximal expansion, while MyoII accumulated during contact contraction and peaked just prior to maximal contraction, consistent with previous reports (Del Signore et al., 2018; Malin et al., 2022). In *pten* mutant eyes, the positive correlation between F-actin accumulation and contact length decreased significantly compared with WT (Fig. 3E-F, I). Additionally, the negative correlation between MyoII and contact length decreased as well (Fig. 3G-H, J). Moreover, the pulse amplitude of F-actin decreased, although the pulse amplitude of MyoII was not significantly different from WT (Fig. 3K-L). During periods of contraction, the parallel cables of MyoII that form along the LC-LC contacts were frequently further apart than in WT, suggesting that these contacts were either under greater tension,

reduced protrusion, or both (Fig. 3C-D, red arrows). Because contractile and protrusive dynamics are mutually dependent in this system, disrupting the regulation of one network may disrupt the other. The reduction in actin pulsing leads us to hypothesize the more direct effect may be on F-actin branching and protrusive force. Overall, we find that *pten* affects both protrusive F-actin branching and contractile MyoII dynamics, supporting a role for *pten* in rebalancing the opposing forces generated by these networks during epithelial remodeling.

pten affects the localization and dynamics of protrusive and contractile regulators at LC-LC contacts

The disruption of protrusive F-actin and contractile MyoII dynamics in *pten* mutant eyes may arise from the disruption of the WRC, which regulates F-actin branching, or Rho1 GTPase signaling, which regulates actomyosin contractility, or from the disruption of both. The persistent accumulation of MyoII and the diminished accumulation of F-actin along the LC-LC suggested that F-actin assembly is affected. We therefore examined the dynamic accumulation of the WRC subunit Abi, which activates Arp2/3-mediated F-actin branching, at the LC-LC contacts of *pten* mutant eyes compared with WT (Fig. 4A-B, Movie 4). To monitor WRC dynamics, we engineered an Abi protein that is GFP-tagged (GFP::Abi) and controlled by the ubiquitin promoter (Akbari et al., 2009). We found strong pulse amplitudes of Abi at vertices during contact expansion in WT and significantly decreased pulse amplitudes and frequencies in *pten* mutant eyes (Fig. 4C-D). The correlation between contact length and Abi levels at vertices was also decreased in *pten* eyes compared to WT (Fig. 4E-G). These results highlight the crucial role of the WRC at tAJs in controlling the dynamics of F-actin branching and protrusive force generation. It suggests that the defects in length pulsing, at least in part, arise from defects in WRC accumulation and activation of F-actin branching at tAJs.

The diminished amplitude of contact expansion may also arise from increased contraction. To distinguish between these possibilities, we measured the initial recoil velocities of vertices after ablation of a small region in the middle of single LC-LC contacts in WT and *pten* mutant eyes as a proxy for the tension these contacts hold (Colombelli and Solon, 2013; Rauzi and Lenne, 2015) (Fig 4H-I, Movie 5). We found no difference between WT and *pten* mutant eyes in the recoil velocities of LC-LC contacts, indicating that *pten* loss does not increase tension at LC-LC contacts (Fig. 4J-L). It

implies that Pten primarily promotes WRC activation and F-actin branching to support protrusive dynamics and contact expansion.

Pten's lipid phosphatase activity is required for epithelial remodeling

Because of prior research implicating PIP_3 in epithelial remodeling, and the nature of the *pten*^{c494} allele, which inactivates Pten's phosphatase activity, we hypothesized that Pten's effects on the epithelium were mostly due to its lipid phosphatase function (Bardet et al., 2013; Del Signore et al., 2018; Di Paolo and De Camilli, 2006; Huang et al., 1999). Point mutants of vertebrate PTEN (C124S and G129E) were previously shown to impair both its lipid and protein phosphatase activity or preferentially only its lipid phosphatase activity, respectively (Liliental et al., 2000; Myers et al., 1998; Qi et al., 2020). We introduced the equivalent point mutations (C132S and G137E, respectively) in *Drosophila* Pten to determine if Pten modulates PIP_3 dynamics to control epithelial remodeling. We then used the MARCM technique to express each variant in *pten* mutant clones to determine if they could rescue the *pten* clonal phenotypes. We found that the WT Pten transgene rescued the *pten* clonal phenotypes, while neither the *pten*^{C132S} nor the *pten*^{G137E} point mutant was able to rescue these phenotypes (Fig. S1A-E, G). However, the clonal phenotypes were more severe in the *pten* clones expressing the *pten*^{C132S} variant lacking both the lipid and protein phosphatase activity suggesting that Pten's protein phosphatase activity makes an additional contribution to Pten function in epithelial remodeling (Fig. S1C-D, G). Additionally, even the catalytically dead *pten*^{C132S} variant accomplished minimal rescue when compared to eyes in which no *pten* transgene was expressed at all, suggesting that Pten may have an additional non-catalytic function in the process (Fig. S1D, G). Taken together, our results indicate that Pten's lipid phosphatase activity is essential for eye epithelial remodeling but suggest additional roles for other functions of Pten, including its protein phosphatase activity, in this process.

Pten affects PIP_3 dynamics

Since we found that Pten's lipid phosphatase activity is required for proper epithelial remodeling, we examined

Pten's effects on PIP_3 in developing eyes. We employed the PH domain of Grp1 fused to GFP (Grp1-PH::GFP or GPH) to monitor PIP_3 in *pten* mutant clones and entire eyes (Britton et al., 2002). As expected, we found elevated levels of PIP_3 in *pten* mutant clones compared with WT cells (Fig. 5A). To avoid confounding non-autonomous effects, we compared PIP_3 dynamics in WT eyes with fully mutant *pten* eyes. Similar to WRC pulses, PIP_3 pulses and contact expansion pulses co-occurred in WT eyes (Fig. 5B, Movie 6). We found decreased pulse amplitude and increased pulse frequency of PIP_3 in the *pten* mutant eyes (Fig. 5C-E, Movie 6). Moreover, the positive correlation between PIP_3 and contact length was abolished in the mutant eyes. In WT eyes, the correlation between PIP_3 and contact length peaked at an average time shift of -3 minutes, while in *pten* mutant eyes there was a much lower correlation and no such peak (Fig. 5F-I). Thus, PIP_3's predictable pulsed dynamics were eliminated in *pten* mutant eyes and it remained constitutively high and mostly static.

Pi3K affects eye epithelial remodeling

To further determine how Pten regulates PIP_3 dynamics to affect epithelial remodeling, we examined the role of Pi3K, the enzyme that phosphorylates PIP_2 to PIP_3, in this process. We asked whether increasing Pi3K activity could mimic the phenotype of *pten* mutants and if the loss or downregulation of Pi3K function affects epithelial remodeling. Active Pi3K consists of a catalytic subunit, Pi3K92E (Pi3K-cat), and a regulatory subunit, Pi3K21B (Pi3K-reg) (Leevers et al., 1996; Weinkove et al., 1997). To increase Pi3K activity, we expressed a constitutively active, membrane-tethered variant of Pi3K-cat (PI3K-cat.CAAX) (Leevers et al., 1996). As eyes and clones mutant for *Pi3K-reg* were very small and challenging to interrogate, we used a combination of a *Pi3K-reg* deletion mutant generated using CRISPR-based genomic engineering and eyes and clones depleted of Pi3K-cat using RNA-mediated interference (RNAi) (Trivedi et al., 2020). We confirmed the increase or reduction of Pi3K function by monitoring PIP_3 levels with GPH in Pi3K-cat.CAAX- and Pi3K-cat RNAi-expressing clones as well as clones mutant for *Pi3K-reg* (Fig. S2A-C, K-L). We found that increasing the function of Pi3K-cat led to pinched contacts and defects similar to those found in *pten* mutant eyes, such as rosettes and clustered bristles. However, the aberrant 1°-1° contacts common in *pten* mutant eyes were relatively rare (Fig. S2A, D, K).

Depleting the function of Pi3K-cat also led to defects in epithelial remodeling, with some defect types also found in *pten* mutants, such as rosettes and aberrant 1°-1° contacts (Fig. S2E, L). Similar defects were also found in *Pi3K-reg* mutant eyes (Fig. S2F).

As both the increase and decrease of Pi3K and PIP_3 levels cause defects in cytoskeletal regulation, we examined PIP_3 dynamics in clones with increased and decreased Pi3K activity. We found that PIP_3 pulsing and correlation with contact length were reduced in Pi3K-cat.CAAX clones (Fig. 6A-B, Movie 7). Very low overall levels of PIP_3 in Pi3K-depleted clones made quantifying dynamics problematic, but fluctuations of PIP_3 appeared reduced in these as well (Supplemental Fig. S2J, Movie 7). We additionally measured the overall amplitude of contact length pulsing in these clones as well as in eyes fully mutant for *PI3K-reg*. The amplitude of contact length pulsing was reduced in the mutants compared to WT, and, although the severity of the phenotype varied from clone to clone, showed a trend toward reduction in both PI3K.CAAX- and PI3K RNAi-expressing clones (Fig. 6C-D, supplemental Fig. S2K-M). In addition, we observed a possible association between Pi3K activity and E-cad, with higher levels of Pi3K expression seemingly leading to higher E-cad levels, although the effect was variable (Supplemental Fig. S2K-L).

To further characterize the *Pi3K* loss-of-function phenotype, we examined the dynamics of F-actin, MyoII, and the WRC in eyes mutant for *Pi3K-reg* (Movie 8). Similar to *pten* mutant eyes, we found a reduction in correlations between contact length and the WRC (Fig 6E) as well as with F-actin and MyoII (Fig. 6F). Finally, to further test Pten's relationship with Pi3K, we generated *pten* mutant clones expressing RNAi for Pi3K-cat. Depleting *Pi3K* function partially rescued the *pten* epithelial phenotype, further indicating a role for PIP_3 in this process (Supplemental Fig. S1F-G). Taken together, these results demonstrate a role for Pi3K in regulating force generation and transmission and raise the possibility that precise modulation of PIP_3 cycling, in addition to overall levels, is required for proper epithelial remodeling.

Pten affects Rac1 function while Rac1 affects PIP_3 and protrusive dynamics

Because *pten* mutants disrupt PIP_3, WRC, and protrusive dynamics and because Rac1 and PIP3 are known to activate the WRC *in vitro* and in cell systems, we tested the role of Rac1 in this process (Fig. 7A-B, Movie 9). We found that the amplitude and frequency of Rac1 fluctuations were reduced compared with WT, indicating impaired dynamics (Fig. 7C-D). Additionally, we found a slight but significant positive correlation between GFP-tagged Rac1 and LC-LC contact length in WT. This correlation appeared to be abolished in *pten* mutants (Fig. 7E-G).

It was previously shown that eyes mutant for both *rac1* and *rac2* have defects in epithelial organization (Martin-Bermudo et al., 2015). Considering this role of *rac* genes and their potential interaction with *pten*, we overexpressed Rac1 and investigated its effects on epithelial remodeling. Broad Rac1 expression resulted in epithelial remodeling defects and altered mechanical and cytoskeletal dynamics. The apical area of epithelial cells was enlarged and dynamically expanding and relaxing, in contrast to the static, pinched LC-LC contacts observed in *pten* eyes. While in WT, PIP_3, Abi, and F-actin are dynamically enriched at vertices and LC-LC contacts, in Rac1 expressing eyes they concentrated more strongly at vertices and additionally localized along the entire cell perimeter at the level of apical AJs. Moreover, PIP_3 accumulated in pulses along the apical cell area, implying that Rac1 may activate Pi3K. Together, these effects strongly suggest that Rac1 and PIP_3 activate the WRC and protrusive F-actin dynamics in part through the activation of Pi3K through a positive feedback mechanism (Fig. 7H-J, Movie 10). The expansion of the LCs often led to cell overexpansion and tears of the epithelium that coincided with waves of PIP_3, Abi and F-actin along the overexpanding cell perimeter (Supplemental Fig. 3A-C, Movie 11).

Clonal overexpression of Rac1 induced similar epithelial tears and fused cells (Supplemental Fig. 3D). When we overexpressed Rac1 in *SCAR* mutant clones, we observed a smaller number of ruptured cells, with fewer than half the eyes observed exhibiting this phenotype. Expressing Rac1 in *pten* clones caused a similarly reduced frequency of eyes containing ruptures. These results may suggest that Rac1 acts at least partially through the WRC to promote protrusive F-actin dynamics and apical area expansion, and that proper PIP_3 dynamics are needed for Rac1 to function. However,

cell survival also appeared reduced in *SCAR* and *pten* clones compared to WT Rac1 overexpression clones, so this experiment cannot exclude the alternate explanation that reduced ruptures were simply a result of reduced cell survival.

Overall, our findings show Pi3K dynamics are needed to promote Rac1 function, which in turn influences WRC activation, F-actin branching, and protrusive force generation. In addition to activating the WRC and protrusive dynamics indirectly through Rac1, PIP_3 dynamics could also activate the WRC directly and thus synergize with Rac1 to maximally activate the WRC. Rac1 also appears to sustain and amplify the PIP_3 signal, possibly through Pi3K activation, to robustly assemble a protrusive branched F-actin network to drive the pulsatile LC-LC contact expansion.

Pten and Pi3K localize dynamically in the vicinity of the LC-LC contacts

If Pi3K and Pten affect the pulsing of the LC-LC contacts, we would expect them to localize either to or near the LC-LC contacts and the associated tAJs. Pi3K-reg is primarily responsible for the spatiotemporal control of Pi3K activation (Fruman, 2010). Therefore, to examine the sites of Pi3K activation, we generated a GFP-tagged Pi3K-reg (Pi3K-reg::GFP) driven by the ubiquitin promoter. We found that Pi3K-reg::GFP localized to apical cell contacts at the level of AJs where it accumulated in a dynamic pattern. During early expansion, Pi3K-reg::GFP localized to four spots on either side of tAJs. As the contacts expanded, the domain of Pi3K-reg localization expanded and moved toward the tAJs (Fig. 8A, Movie 12). To quantify this, we measured the temporal cross-correlation between Pi3K at or adjacent to the vertices and overall contact length and found that the adjacent-to-vertex correlation peaked earlier than the at-vertex correlation (Fig. 8B). Pi3K both at and adjacent to the vertex correlated strongly with F-actin (Fig. 8C). Therefore, Pi3K could mediate the expansion of the LC-LC contact by promoting protrusive dynamic adjacent to the tAJs to push the plasma membrane outward. To further investigate this process, we used immunostaining to examine Pi3K-reg::GFP localization relative to E-cad and Sdk, a tAJ-specific adhesion protein previously implicated in epithelial force balancing (Malin et al., 2022). When Pi3K localized in spots around the tricellular junctions, it colocalized strongly with E-cad. Less commonly, it localized with Sdk at the tricellular junction itself, though in some cases the strongest concentrations of Sdk and Pi3K-reg were directly adjacent to each other and partially but not fully overlapping. Many contacts were also asymmetrical with

respect to Pi3K localization at the tAJs (Fig. 8D).

Pten activation is mediated by membrane localization, which requires its PDZ domain binding motif and interaction with phospholipids (Das et al., 2003; Jang et al., 2021). We created a GFP::Pten reporter driven by the ubiquitin promoter to monitor Pten localization in order to identify the membrane sites where Pten counteracts Pi3K. We specifically tagged the Pten2 isoform, which contains the C-terminal PDZ domain-binding motif that has been previously shown to localize Pten to apical junctions (Maehama et al., 2004; Pickering et al., 2013; von Stein et al., 2005). We found that GFP::Pten accumulated in a diffuse pattern both at and surrounding the LC-LC contacts (Fig. 8E, Movie 12). Although Pten localization was dynamic and correlated with F-actin levels, Pten levels were relatively constant during both contact expansion and contraction (Fig. 8F-G). Taken together, these localization dynamics suggest that PIP_3 levels are primarily regulated by fluctuations in Pi3K levels at apical junctions, while PIP_3 turnover is regulated by both Pi3K and Pten.

DISCUSSION

After the initial cellular organization of ommatidia through the cell-specific distribution of adhesion molecules, continuous movement of cells is required for the mature precise geometry of the eye to develop. Regular pulses of contraction and expansion of cell contacts are characteristic of this movement. Here, we show that Pten and Pi3K regulate oscillating levels of PIP_3 at apical junctions and this is necessary for normal pulsing shape changes and morphogenesis. The function of PIP_3 is to generate protrusive force and elongate contacts by recruiting the WRC and thereby promoting branched F-actin. The dependence of protrusion on dynamic changes in PIP_3 combined with the proximity of Pi3K and Pten to each other near junctions makes this system uniquely suited to precise temporal control of protrusion. We provide evidence that phosphoinositides controlled by Pten and Pi3K affect Rac1 function and propose that PIP_3 cooperates with Rac1 to activate the WRC and protrusive F-actin branching to control cytoskeletal and contact length pulsing.

Technical considerations

While phosphoinositides are very widely studied, little of this research relates to planar cell morphogenesis. In addition to looking at cell architecture, we utilized live imaging of reporters for cytoskeletal indicators of both contractile and protrusive forces, as the control of protrusion in planar epithelial development remains largely unexplored. Dynamic imaging of PIP_3 allowed us to quantify its cyclical ebb and flow in addition to simple levels. We used engineered point mutants to differentiate between the lipid phosphatase and protein phosphatase functions of Pten. In addition, we directly investigated Pi3K function using a novel null mutation generated by CRISPR/Cas9 gene editing (Trivedi et al., 2020), and verified the mutation in *Pi3K-reg* by loss of PIP_3 and the associated phenotype. Further, by recombining *Pi3K-reg* with an FRT chromosome, we showed the feasibility of studying Pi3K-null clones. This contrasts with previous work done with relying on dominant-negative suppression of Pi3K function in which residual function or unanticipated effects remain a consideration. Genetic tests for expressing Rac1 in *SCAR* and *pten* mutant clones imply that Pten and SCAR are important for the function of Rac1, implying positive feedback loops with PIP_3 and Pi3K. Taken together these approaches provide new insight into the role of Pten, Pi3K, and PIP_3 in regulating protrusive forces and in turn planar epithelial morphogenesis.

Our results show that cell contacts are pinched and fail to lengthen in *pten* mutants, a result that echoes those of an earlier study of *Drosophila* notum development (Bardet et al., 2013). In that case, the mechanism of this effect was linked to persistent myosin and overactive contractile forces. However, since that time, the importance of protrusive forces in contact remodeling has been demonstrated, including strong pulsatile PIP_3 accumulation coinciding with the accumulation of the WRC and protrusive F-actin (Del Signore et al., 2018; Malin et al., 2022; Patel et al., 2008). This observation aligns with literature linking PIP_3 with activation of the WRC in other contexts (Chen et al., 2017; Hume et al.; Koronakis et al., 2011; Mendoza, 2013; Mendoza et al., 2011; Schaks et al., 2018). Taken together they suggested the hypothesis that the Pten phenotype is caused by dysregulation of protrusive forces, even though the contacts are shortened. Key results supporting this hypothesis in our system are that the WRC does not accumulate in *pten* mutants, there is no evidence for changes in levels of MyoII and, although contacts are pinched, when laser ablated their recoil

velocity does not change, indicating no change in contractile forces. Therefore, our results put Pten's function in planar epithelial morphogenesis in a new light, establishing its role in regulating protrusive forces in this context.

Because Pten has the potential to act through many intermediaries and has known phosphatase activity on both lipids and proteins, investigating its mechanism of action is important. Our results confirm the importance of PIP_3 in this system. Specifically, we show that a *pten* point mutant with a deficient lipid phosphatase function fails to rescue the *pten* phenotype. In addition, we examine the role of Pi3K, which opposes Pten in the cycle of phosphorylation and dephosphorylation that regulates PIP_3 levels. Mutations affecting Pi3K also show epithelial remodeling deficits. Moreover, we show a partial rescue of the *pten* mutant phenotype by perturbing Pi3K's catalytic subunit. Though our results leave open the possibility of other effects through Pten's protein phosphatase activity, they establish the importance of PIP_3 regulation by Pten and Pi3K in the observed phenotypes.

Strikingly, we found that genetic manipulations that either increased or decreased levels of PIP_3 resulted in similar phenotypes. In phenotypes in which PIP_3 levels were constitutively low due to reduced Pi3K activity, contacts were shortened due to a deficit in protrusion. However, with the elevated PIP_3 levels in *pten* mutants or with constitutively active Pi3K, LC-LC contacts were also short or lost, with a decrease of WRC accumulation and consequently branched F-actin at tAJs. This is opposite to what would be expected given the ability of PIP_3 to activate the WRC and induce protrusive dynamics (Chen et al., 2010; Hume et al.; Lebensohn and Kirschner, 2009; Oikawa et al., 2004; Suetsugu et al., 2006). It has been noted in other contexts that there exists continuous turnover of various phosphoinositides and it remains an open question in the field if this turnover is integral to their mechanism of action (Di Paolo and De Camilli, 2006). The current results reveal that high levels of PIP_3 alone are not sufficient for marshaling protrusive forces in this system, and that dynamism of PIP_3 is also critical. Speculatively, this dependence could optimize the sensitivity of the system and its ability to rebalance mechanical forces, as turnover would allow the balance of different phosphoinositides to rapidly shift. Alternatively, the mechanisms needed for proteins to continuously regenerate their activity in the ongoing process of remodeling actin networks may intrinsically require phosphoinositide levels to fluctuate.

In contracted contacts under high tension, Pi3K-reg localizes at four spots directly adjacent to the tAJs, and PIP_3 levels are low, indicating low Pi3K lipid-kinase activity. During expansion, Pi3K-reg's localization spreads away from these spots, concentrating at tAJs as PIP_3 levels peak. Thus, Pi3K-reg's distribution, as well as its lipid kinase function, change with tension. Pten, in contrast, does not detectably shift distribution through the pulse cycle, but its levels increase with increasing F-actin. The specific mechanisms that regulate Pi3K and Pten distribution here are unknown, but the proteins are clearly correlating with oscillations in mechanical forces. Likewise, during pulsing, Sdk concentrates at tAJs in response to tension and associates with the WRC to reduce tension and promote contact expansion. Pyd, on the other hand, accumulates following maximal contact expansion to increase tension and promote contraction (Malin et al., 2022). Pi3K and Pten join Sdk and Pyd as elements that change in response to pulsing and are moreover molecular effectors of mechanical forces that generate pulsing. Thus, Pi3K and Pten appear as integral components to the feedback loops that generate and maintain pulsing shape changes.

Although they exhibit different patterns of distribution that vary with the pulse cycle, both Pi3K and Pten are enriched at and near a subset of cell-cell contacts at the level of tAJs. The spatial proximity between the two proteins is consistent with their capacity to exert temporally specific control of PIP_3. This is an interesting contrast with other systems in which Pi3K and Pten do not colocalize but are rather separated to define distinct subcellular domains. During epithelialization, Pten localizes apically, while Pi3K localizes basolaterally, and their separate distributions have localized effects to define the apicobasal axis (Martin-Belmonte et al., 2007; Pinal et al., 2006; von Stein et al., 2005). In motile cells, Pi3K localizes to the leading lamellipodium edge while Pten is at the rear and sides to coordinate protrusive with contractile dynamics (Funamoto et al., 2002; Iijima et al., 2002). Thus, the proximity of the Pi3K and Pten proteins at apical junctions positions them for precise temporal regulation of PIP_3 pulsatile dynamics in this specific location.

Our data support the idea that PIP_3 regulates the WRC both directly and at least in part indirectly through Rac1 activation. Loss of *pten* reduces the pulsing of Rac1 levels, suggesting that PIP_3 activates Rac1. This would be consistent with the documented roles of PIP_3 and Rac1 in promoting the formation of lamellipodia and with current models of WRC activation (Chen et al., 2017; Chen et al., 2010; Ridley et al., 1992). We also found that overexpressing Rac1 induced

protrusive F-actin and PIP_3 accumulation causing expansion of cells' apical area, even to the point of rupture. This is an interesting contrast to manipulations that raised PIP_3 levels directly that did not result in excess protrusion. Taken together these data suggest the hypothesis that PIP_3 could activate both a GEF and a GAP for Rac1 at apical junctions and that Rac1 itself might then activate Pi3K to sustain its activation and generate a pulse of WRC activation and F-actin branching (Kovacs et al., 2002; Nakagawa et al., 2001; Perez et al., 2008). Thus, Rac1 could act not only as an effector of PIP_3 in activating the WRC, but also a feedback amplifier of PIP_3 signaling and through these actions together would have the capacity to robustly promote F-actin branching at apical junctions.

In sum, we show that Pten and Pi3K affect PIP_3 pulsing in a manner necessary to control cytoskeletal and mechanical pulsing. Characterization of multiple genetic conditions indicates that dynamic changes in PIP_3 levels are essential for promoting protrusion. PIP_3 pulsing activates the WRC and F-actin branching, and this system utilizes Rac1 to promote protrusive dynamics and reinforce PIP_3 production through positive feedback. Additionally, Pten levels and both the distribution and the activity of Pi3K are regulated with cycles of contact expansion and contraction, suggesting regulation by mechanical signals. Taken together these results reveal the importance of Pten, Pi3K and PIP_3 in generating protrusive forces at tAJs in a process that is essential for planar epithelial morphogenesis.

ACKNOWLEDGEMENTS

We thank E, Hafen, Daniel St Johnston, T. Millard, R. Padinjat, F. Pichaud, A. Martin, and J. Zallen for generous gifts of fly strains, the Bloomington Stock Center, the Vienna *Drosophila* Research Center, and the Kyoto Stock Center for fly stocks, and the Developmental Studies Hybridoma Bank for antibodies, G. Rong and the Institute for Chemical Imaging of Living System (CILS) at Northeastern University for access and assistance with multi-photon confocal imaging. We thank K. G. Commons for critical reading of the manuscript. This work was supported by grants from the National Institute of Health to V.H. (R01 GM129151).

METHODS

Fly strains

To examine the *pten* loss-of-function phenotypes, we employed the *pten*^{c494}, *pten*^{3}, and *pten*^{L2100} alleles recombined to an FRT40A site to generate genetically marked mutant clones and fully mutant eyes. We used *pten*$^{C494/3/L2100}$ FRT40A; α-Cat::Venus^{CPTI} to examine *pten*'s role in epithelial rearrangements and *pten*^{3} FRT40A combined with cytoskeletal reporters to examine *pten*'s role in cytoskeletal control. To determine if Pten's lipid phosphatase or protein phosphatase activity affects epithelial remodeling, we constructed UAS-GFP::Pten2 (C132S), a point mutant that affects both the protein phosphatase and lipid phosphatase activities, UAS-GFP::Pten2 (G137E), a point mutant that preferentially disrupts the lipid phosphatase activity, and WT UAS-Pten2::GFP. We selected UAS insertions on the third chromosome with similar expression levels to determine if these variants can rescue the *pten* clonal phenotypes using the MARCM technique. To examine Pten and Pi3K-reg protein distribution and dynamics, we employed UAS-GFP::Pten2 and constructed a Ubi-GFP::Pten and Ubi-Pi3K-reg::GFP. Additionally, we constructed Ubi-GFP::Abi to track the dynamics of the WRC.

Fly lines from the Bloomington *Drosophila*: (1) UAS-Lifeact::Ruby, (2) *sqh*^{AX3}/FM7c*;* sqh-Sqh::GFP, (3) tGPH; *Sb/TM3*, (4) tGPH (III), (5) Rac1-GFP::Rac1 (III), (6) *y w*, UAS-Pi3K92E.CAAX, (7) UAS-Pi3K92E RNAi, (8) UAS-Rac1, (9) GMR-GAL4, (10), Ey-GAL4, (11) UAS-dicer (II), (12), UAS-dicer (III), (13) hsFLP (II), (14) Ey-FLP (II), (15) GMR-Hid FRT40A /Cyo-GFP; Ey-GAL4 UAS-FLP, (16) *w* Ey-FLP; GMR-myrRFP FRT40A, (17) *y w* hsFLP; GMR-myrGFP FRT40A FRT, and (18) pw+ 21C, pw+ 36F, FRT40A. α-Cat::Venus^{CPTI002596} was obtained from the Kyoto stock center.

Fly lines previously described by Del Signore et. al. (2018): (1) GMR-GAL4, α-Cat::Venus, (2) UAS-Lifeact::Ruby; GMR-GAL4. Additional stocks used: (1) sqh-UtrABD::GFP and (2) sqh-UtrABD::GFP, sqh-Sqh::mCherry (gift of A. Martin), (4) ubi-Ecad::GFP (5) Shg-Shg::mCherry ; tGPH (6) Ey-GAL4 ; UAS-dicer (7) UAS-dicer ; GMR-GAL4.

The following stocks were gifts as indicated: *pten*^{3} 40A FRT and *pten*^{2L100} 40A FRT (E. Hafen), *pten*^{c494} FRT 40A (D. St Johnston), *PiK21B*$^{\Delta}$ indels (2,9) (3,2), (3,6) (P. Raghu). A *Pi3K21B*$^{\Delta 2,9}$ FRT40A recombinant was created using indel (2,9).

Fly lines that were generated in this study: 1) FRT40A pten^{3}; α-Cat::Venus, 2) pten^{3} FRT40A; Ubi-Abi::GFP, 3)

pten^{3} FRT40A; Sqh-Sqh::GFP, 4) *pten^{3}* FRT40A; Sqh-Utr::GFP, 5) *pten^{3}* FRT40A; tGPH, 6) *pten^{3}* FRT40A; Rac1-GFP::Rac1 (BL-52285), 7) *pten^{3}* FRT40A; UAS-GFP::Pten2, 8) *pten^{3}* FRT40A; UAS-GFP::Pten2^{C132S}, 9) *pten^{3}* FRT40A; UAS-GFP::Pten2^{G137E}, 10) FRT40A ; UAS-GFP::Pten2, 11) *Pi3K21B$^{\Delta 2,9}$* FRT40A, 12) *Pi3K21B$^{\Delta 2,9}$* FRT40A ; a-Cat::Venus, 13) *Pi3K21B$^{\Delta 2,9}$* FRT40A ; Sqh- Utr::GFP, Sqh-Sqh::mCherry, 14) *Pi3K21B$^{\Delta 2,9}$* FRT40A ; Ubi-GFP::Abi, 15) *y w*, UAS-Pi3K92E.CAAX (BL-8294) ; Ey-FLP, 16) UAS-Pi3K92E.RNAi (BL-27690) ; hsFLP, 17) ubi-Ecad::GFP ; Act>>GAL4, UAS-RFP, 18) tGPH (BL-8163) ; Act>>GAL4 UAS-RFP, 19) UAS-Rac1 (BL-58816) ; Sqh-Utr::GFP, Sqh-Sqh::mCherry,20) UAS-Rac1 ; tGPH, 21) Sqh-UtrABD::mCh ; GMR-GAL4, ubi-GFP::Abi, 22) SCAR$^{\Delta 37}$ 40AFRT; UAS-Rac1 (BL-28874), 23) *pten^{3}* 40AFRT ; UAS-Rac1, 24) 40AFRT ; UAS-Rac1.

Genetic analysis

GMR-GAL4 and Ey-GAL4 lines were used to broadly express UAS-transgenes in the eye (Wernet et al., 2003). The FLP/FRT (Xu & Rubin, 1995), and the MARCM techniques (Lee and Luo, 2001) were used to generate genetically marked clones by FLP-mediated mitotic recombination. The EGUF technique was used to generate entirely mutant eyes (Stowers and Schwarz, 1999). The Flp-out/GAL4 technique was used to express desired transgenes in genetically marked clones. *y w* Ey-FLP; Ubi-mRFP, FRT40A and *y w* hsFLP; Ubi-GFP, FRT40A were used to generate *pten* or *Pi3K-reg* mutant FLP/FRT clones, Ey-FLP, UAS-GFP; tub-GAL80 FRT40A; tub-GAL4 to generate MARCM clones and GMR-Hid FRT40; Ey-GAL4, UAS-FLP to generate entirely mutant eyes. Mitotic and FLP-out clones were induced by a heat shock for 30 minutes at 34°C.

Molecular biology and construction of genetically encoded reporters

We generated several new reporters driven by the ubiquitin promoter including Ubi-GFP::Pten, Ubi-Pi3K21B::GFP, and Ubi-GFP::Abi, and several UAS-driven transgenes including UAS-GFP::Pten, UAS-GFP::Pten (C132S), and UAS-GFP::Pten (G137E). The *pten* open reading frame (ORF) was amplified from cDNA clone IP16020 (RRID:DGRC_1603573), the Pi3K21B ORF from LD42724 (RRID:DGRC_5517), and the Abi ORF from LD37010

(RRID:DGRC_2550). The PCR products were inserted into pENTR plasmids by TOPO cloning. All expression clones were generated by the Gateway technology (Walhout et al. 2000) using the *Drosophila* Gateway Vector Collections (gift of T. Murphy and C.-Y. Pay) using the Clonase II reaction to fuse the ORFs in frame with a desired fluorescent protein. Site-directed mutagenesis using Agilent Technologies QuickChange II was performed to inactivate both the lipid and protein phosphatase activity of Pten by substituting a cysteine as position 132 to serine to generate UAS-Pten::GFP (C132S) or to inactivate the lipid phosphatase activity only by substituting the glycine at position 137 to glutamine to generate UAS-Pten::GFP (G137E). Ubi-Pi3K-reg::GFP was inserted at the P{CaryP}attP2 site (estimated at 68A4) by PhiC31-mediated recombination. We introduced an AttB site to pUGW using site-directed mutagenesis using New England Biolabs NEB Q5 Site-directed mutagenesis kit (Akbari et al., 2009). Transgenic fly lines carrying these transgenes were established by standard methods by BestGene Inc.

Method detail

Immunofluorescence

White prepupae (0h APF) were selected and aged on glass slides in a humidifying chamber at 25°C. Pupal eyes were dissected in phosphate-buffered saline, fixed for 35 minutes in 4% paraformaldehyde in PBS, and stained with antibodies in PBS with 3% BSA, 0.3% Triton X-100, and 0.01% Sodium Azide. Primary antibodies used were rat anti-E-cad (DSHB #DCAD2, 1:100), mouse anti-Dlg (DSHH #4F3, 1:500), and guinea pig anti-Sdk (Astigarraga et al., 2018). Alexa647 (Molecular Probes) and Cy3 and Cy5 (Jackson ImmunoResearch) conjugated secondary antibodies were used at 1:150.

Sample preparation for live imaging

Pupae were selected and aged as described above. Larvae and pupae expressing UAS-Rac1 were aged at 18°C and then shifted to 30°C 4 hours before imaging to conditionally increase transgene expression. Image data were collected on an LSM800 laser scanning confocal microscope. Live imaging of pupal eyes was conducted as previously described (Del Signore et al., 2018). Prior to imaging, the operculum and surrounding pupal case were peeled carefully

to expose the eyes. Pupae were inserted in a slit created in an agarose block with one eye facing the coverslip. The agarose block was fitted with a custom-made rubber gasket and capped with a custom-built humidified chamber.

Confocal imaging

For analysis of epithelial remodeling and protein dynamics, an image stack was obtained every 1 minute unless otherwise noted with pinhole size=1 AU using a 63X, 1.4 NA, plan Apochromat oil immersion objective, 0.7 □m per optical section with a 10-50 % overlap between sections, at a scan speed of 7 without averaging.

Laser nano-ablation

Laser nano-ablations to measure bond tension were performed using a Zeiss LSM880 NLO with a near-infrared InSight X3 multi-photon tunable laser (680-1300nm) using a 740nm multiphoton excitation. Samples were imaged with α-Cat::Venus to identify the junctions for ablation using a 63X oil immersion objective (N.A 1.4). A small field size, of 1x8 pixels, was ablated in the center of LC-LC contacts using a 30-40% laser output, at a scan speed of one, with one iteration. Images were collected every 0.5 seconds for 120 seconds and ablations were performed 3 seconds after the beginning of each experiment. To determine the initial recoil velocity ($V_{max)}$), we measured the distance between vertices of the ablated cell-cell contacts in Fiji and plotted them as a function of time using Prism 9 (GraphPad). V_{max} was determined using fitting function f(t) as follows: $f(t) = A \cdot (1\text{-}e^{-t/\tau})$ and $V_{max} = df(0)/dt = A/\tau$ where A is the total retraction amplitude and τ the decay rate constant.

Quantification and Statistical Analysis

Quantitative assessment of eye phenotypes

We processed images and counted features using Fiji. We created Regions of Interest (ROIs) in the center of retinas in which to count cellular defects. Then we used the Cell Counter tool to count defects within the area. In addition, we counted the total number of edges, vertices, and ommatidia within the ROI. The following defects were

normalized to the number of edges: 1) A missing LC, defined as any edge with only one bristle and one lattice cell, or two lattice cells and no bristles. 2) A separation, defined as any edge along which 1° cells from two different ommatidia were in direct contact. 3) An extra LC, defined as any edge with more than three lattice cells, or two bristles and more than two LCs. The following defects were normalized to the number of vertices: 1) A rosette, defined as a bristle with four LCs contacting it instead of the normal three. 2) A missing 3° LC, defined as a vertex at which a 3° LC was missing and where a contact between multiple secondary cells was formed. 3) A misplaced bristle, defined as an edge with a bristle in the middle. Statistical differences between conditions were examined using a Chi-Square Test. For counting numbers of rosettes in FLP/FRT and MARCM clones, a vertex was considered WT if the vertex and all adjacent secondary cells were WT, mutant if all cells were mutant, and mixed otherwise.

Analysis of contact dynamics

We examined contact dynamics at ~28h APF at the end of the pruning stage, when some, but not all, ommatidial edges had 2 or more 2° cells. Individual LC-LC contacts along horizontal edges were traced manually at 1-minute intervals for 60 minutes using a Fiji plugin with a line segment selection producing 40-60 ROIs per contact. A custom Fiji "Junction Analyzer" script measured the length of each ROI. Then, a Python script operating on the extracted length values calculated the features of the pulsing. The data were smoothed using a Gaussian filter with sigma=2. Pulse amplitudes were taken using the absolute value of the difference between adjacent local maxima and minima. This value was divided by the average contact length to get the normalized amplitude. Pulse frequencies were taken using the number of minutes between maxima. Values for a given contact were averaged to produce an average amplitude or frequency per contact. Statistics were performed on average amplitudes and frequencies per contact using a Kruskal-Wallis test with Dunn's Multiple Comparison test in Prism (Version 9.5.0).

Time-shifted Pearson's correlation analysis

Contact dynamics were analyzed by manual tracing with a line segment selection (width=5px). Vertices were automatically placed at both ends of these line segments as circular ROIs (diameter=6px). Contact length, pixel mean, and total intensity and background for each channel at each time point were collected using the Junction Analyzer Fiji macro. For Sqh::GFP, Rac1::GFP, and GFP::Pten2, and Grp1-PH::GFP (GPH), analysis was based on the mean intensity over the full contact length, while for Utr::GFP, GFP::Abi, and Pi3K-reg::GFP, it was based on the mean intensity at the vertices. Time-resolved Pearson's cross-correlations (time windows from +/-19 minutes) were compared between the mean fluorescent marker intensities and contact length using 40-60 min long movies and calculated using a custom Python script along with packages NumPy and SciPy. Data presented are the average Pearson's correlations of individual contacts as noted in figure legends and are presented as the mean correlation (R) +/- SD. A one-sample t-test was used to calculate whether average Pearson R-values and time shifts were significantly different from zero. To calculate whether the peak average R-value differed from the average R-value at a time shift of 0, a paired t-test was used. An unpaired t-test was used for comparisons between groups to analyze normally distributed data, while the Mann-Whitney *u* test was used to analyze non-normally distributed data.

Quantification of contact polarity in Rac1 overexpression eyes

Pupae were aged for ~48h at 18C and then transferred to 25C for 4-6h, for an effective age of 26-27h APF. Levels of reporters at tAJs were measured in Fiji by averaging the mean intensity at two circular ROIs of size 12, one placed at each vertex. Levels of reporters at bAJs were measured using a single circular ROI, defaulting to size 12 but reduced in size if necessary to avoid overlapping with the tAJ ROIs. We then took the ratio between the intensity at tAJs and bAJs. Comparisons between genotypes were performed with an unpaired t-test for normally distributed data and a Mann-Whitney *u* test for non-normally distributed data.

LITERATURE CITED:

Akbari, O.S., D. Oliver, K. Eyer, and C.Y. Pai. 2009. An Entry/Gateway cloning system for general expression of genes with molecular tags in *Drosophila melanogaster*. *BMC Cell Biol*. 10:8.

Astigarraga, S., J. Douthit, D. Tarnogorska, M.S. Creamer, O. Mano, D.A. Clark, I.A. Meinertzhagen, and J.E. Treisman. 2018. *Drosophila* Sidekick is required in developing photoreceptors to enable visual motion detection. *Development*. 145.

Auger, K.R., L.A. Serunian, S.P. Soltoff, P. Libby, and L.C. Cantley. 1989. PDGF-dependent tyrosine phosphorylation stimulates production of novel polyphosphoinositides in intact cells. *Cell*. 57:167-175.

Bao, S., and R. Cagan. 2005. Preferential adhesion mediated by Hibris and Roughest regulates morphogenesis and patterning in the *Drosophila* eye. *Dev Cell*. 8:925-935.

Bardet, P.L., B. Guirao, C. Paoletti, F. Serman, V. Leopold, F. Bosveld, Y. Goya, V. Mirouse, F. Graner, and Y. Bellaiche. 2013. PTEN controls junction lengthening and stability during cell rearrangement in epithelial tissue. *Dev Cell*. 25:534-546.

Blackie, L., M. Tozluoglu, M. Trylinski, R.F. Walther, F. Schweisguth, Y. Mao, and F. Pichaud. 2021. A combination of Notch signaling, preferential adhesion and endocytosis induces a slow mode of cell intercalation in the *Drosophila* retina. *Development*. 148.

Blackie, L., R.F. Walther, M.F. Staddon, S. Banerjee, and F. Pichaud. 2020. Cell-type-specific mechanical response and myosin dynamics during retinal lens development in *Drosophila*. *Mol Biol Cell*. 31:1355-1369.

Britton, J.S., W.K. Lockwood, L. Li, S.M. Cohen, and B.A. Edgar. 2002. *Drosophila*'s insulin/PI3-kinase pathway coordinates cellular metabolism with nutritional conditions. *Dev Cell*. 2:239-249.

Cagan, R. 2009. Principles of *Drosophila* eye differentiation. *Curr Top Dev Biol*. 89:115-135.

Cagan, R.L., and D.F. Ready. 1989. The emergence of order in the *Drosophila* pupal retina. *Dev Biol*. 136:346-362.

Cantley, L.C. 2002. The phosphoinositide 3-kinase pathway. *Science*. 296:1655-1657.

Carthew, R.W. 2007. Pattern formation in the *Drosophila* eye. *Curr Opin Genet Dev*. 17:309-313.

Chalhoub, N., and S.J. Baker. 2009. PTEN and the PI3-kinase pathway in cancer. *Annu Rev Pathol*. 4:127-150.

Chan, E.H., P. Chavadimane Shivakumar, R. Clement, E. Laugier, and P.F. Lenne. 2017. Patterned cortical tension mediated by N-cadherin controls cell geometric order in the *Drosophila* eye. *Elife*. 6.

Chen, B., H.T. Chou, C.A. Brautigam, W. Xing, S. Yang, L. Henry, L.K. Doolittle, T. Walz, and M.K. Rosen. 2017. Rac1 GTPase activates the WAVE regulatory complex through two distinct binding sites. *Elife*. 6.

Chen, Z., D. Borek, S.B. Padrick, T.S. Gomez, Z. Metlagel, A.M. Ismail, J. Umetani, D.D. Billadeau, Z. Otwinowski, and M.K. Rosen. 2010. Structure and control of the actin regulatory WAVE complex. *Nature*. 468:533-538.

Colombelli, J., and J. Solon. 2013. Force communication in multicellular tissues addressed by laser nanosurgery. *Cell Tissue Res*. 352:133-147.

Das, S., J.E. Dixon, and W. Cho. 2003. Membrane-binding and activation mechanism of PTEN. *Proc Natl Acad Sci U S A*. 100:7491-7496.

Del Signore, S.J., R. Cilla, and V. Hatini. 2018. The WAVE Regulatory Complex and Branched F-Actin Counterbalance Contractile Force to Control Cell Shape and Packing in the *Drosophila* Eye. *Dev Cell*. 44:471-483 e474.

Devergne, O., K. Tsung, G. Barcelo, and T. Schupbach. 2014. Polarized deposition of basement membrane proteins depends on Phosphatidylinositol synthase and the levels of Phosphatidylinositol 4,5-bisphosphate. *Proc Natl Acad Sci U S A*. 111:7689-7694.

Di Paolo, G., and P. De Camilli. 2006. Phosphoinositides in cell regulation and membrane dynamics. *Nature*. 443:651-657.

Fruman, D.A. 2010. Regulatory subunits of class IA PI3K. *Curr Top Microbiol Immunol*. 346:225-244.

Funamoto, S., R. Meili, S. Lee, L. Parry, and R.A. Firtel. 2002. Spatial and temporal regulation of 3-phosphoinositides by PI 3-kinase and PTEN mediates chemotaxis. *Cell*. 109:611-623.

Galy, A., A. Schenck, H.B. Sahin, A. Qurashi, J.A. Sahel, C. Diebold, and A. Giangrande. 2011. CYFIP dependent actin remodeling controls specific aspects of *Drosophila* eye morphogenesis. *Dev Biol*. 359:37-46.

Gao, X., T.P. Neufeld, and D. Pan. 2000. *Drosophila* PTEN regulates cell growth and proliferation through PI3K-dependent and -independent pathways. *Dev Biol*. 221:404-418.

Goberdhan, D.C., N. Paricio, E.C. Goodman, M. Mlodzik, and C. Wilson. 1999. *Drosophila* tumor suppressor PTEN controls cell size and number by antagonizing the Chico/PI3-kinase signaling pathway. *Genes Dev*. 13:3244-3258.

Hayashi, T., and R.W. Carthew. 2004. Surface mechanics mediate pattern formation in the developing retina. *Nature*. 431:647-652.

Heer, N.C., and A.C. Martin. 2017. Tension, contraction and tissue morphogenesis. *Development*. 144:4249-4260.

Huang, H., C.J. Potter, W. Tao, D.M. Li, W. Brogiolo, E. Hafen, H. Sun, and T. Xu. 1999. PTEN affects cell size, cell proliferation and apoptosis during *Drosophila* eye development. *Development*. 126:5365-5372.

Hume, P.J., D. Humphreys, and V. Koronakis. WAVE regulatory complex activation. *Methods Enzymol*. 540:363-379.

Iijima, M., Y.E. Huang, and P. Devreotes. 2002. Temporal and spatial regulation of chemotaxis. *Dev Cell*. 3:469-478.

Jang, H., I.N. Smith, C. Eng, and R. Nussinov. 2021. The mechanism of full activation of tumor suppressor PTEN at the phosphoinositide-enriched membrane. *iScience*. 24:102438.

Johnson, R.I. 2021. Hexagonal patterning of the *Drosophila* eye. *Dev Biol*. 478:173-182.

Johnson, R.I., A. Sedgwick, C. D'Souza-Schorey, and R.L. Cagan. 2011. Role for a Cindr-Arf6 axis in patterning emerging epithelia. *Mol Biol Cell*. 22:4513-4526.

Johnson, R.I., M.J. Seppa, and R.L. Cagan. 2008. The *Drosophila* CD2AP/CIN85 orthologue Cindr regulates junctions and cytoskeleton dynamics during tissue patterning. *J Cell Biol*. 180:1191-1204.

Koronakis, V., P.J. Hume, D. Humphreys, T. Liu, O. Horning, O.N. Jensen, and E.J. McGhie. 2011. WAVE regulatory complex activation by cooperating GTPases Arf and Rac1. *Proc Natl Acad Sci U S A*. 108:14449-14454.

Kovacs, E.M., R.G. Ali, A.J. McCormack, and A.S. Yap. 2002. E-cadherin homophilic ligation directly signals through Rac and phosphatidylinositol 3-kinase to regulate adhesive contacts. *J Biol Chem*. 277:6708-6718.

Lebensohn, A.M., and M.W. Kirschner. 2009. Activation of the WAVE complex by coincident signals controls actin assembly. *Mol Cell*. 36:512-524.

Lee, T., and L. Luo. 2001. Mosaic analysis with a repressible cell marker (MARCM) for *Drosophila* neural development. *Trends Neurosci*. 24:251-254.

Leevers, S.J., D. Weinkove, L.K. MacDougall, E. Hafen, and M.D. Waterfield. 1996. The *Drosophila* phosphoinositide 3-kinase Dp110 promotes cell growth. *EMBO J*. 15:6584-6594.

Letizia, A., D. He, S. Astigarraga, J. Colombelli, V. Hatini, M. Llimargas, and J.E. Treisman. 2019. Sidekick Is a Key Component of Tricellular Adherens Junctions that Acts to Resolve Cell Rearrangements. *Dev Cell*. 50:313-326 e315.

Li, J., C. Yen, D. Liaw, K. Podsypanina, S. Bose, S.I. Wang, J. Puc, C. Miliaresis, L. Rodgers, R. McCombie, S.H. Bigner, B.C. Giovanella, M. Ittmann, B. Tycko, H. Hibshoosh, M.H. Wigler, and R. Parsons. 1997. PTEN, a putative protein tyrosine phosphatase gene mutated in human brain, breast, and prostate cancer. *Science*. 275:1943-1947.

Liliental, J., S.Y. Moon, R. Lesche, R. Mamillapalli, D. Li, Y. Zheng, H. Sun, and H. Wu. 2000. Genetic deletion of the Pten tumor suppressor gene promotes cell motility by activation of Rac1 and Cdc42 GTPases. *Curr Biol*. 10:401-404.

Maehama, T., N. Kosaka, F. Okahara, K. Takeuchi, M. Umeda, J.E. Dixon, and Y. Kanaho. 2004. Suppression of a phosphatidylinositol 3-kinase signal by a specific spliced variant of *Drosophila* PTEN. *FEBS Lett*. 565:43-47.

Malin, J., C. Rosa Birriel, S. Astigarraga, J.E. Treisman, and V. Hatini. 2022. Sidekick dynamically rebalances contractile and protrusive forces to control tissue morphogenesis. *J Cell Biol*. 221.

Martin-Belmonte, F., A. Gassama, A. Datta, W. Yu, U. Rescher, V. Gerke, and K. Mostov. 2007. PTEN-mediated apical segregation of phosphoinositides controls epithelial morphogenesis through Cdc42. *Cell*. 128:383-397.

Martin-Bermudo, M.D., P.L. Bardet, Y. Bellaiche, and M. Malartre. 2015. The vav oncogene antagonises EGFR signalling and regulates adherens junction dynamics during *Drosophila* eye development. *Development*. 142:1492-1501.

Mendoza, M.C. 2013. Phosphoregulation of the WAVE regulatory complex and signal integration. *Semin Cell Dev Biol*. 24:272-279.

Mendoza, M.C., E.E. Er, W. Zhang, B.A. Ballif, H.L. Elliott, G. Danuser, and J. Blenis. 2011. ERK-MAPK drives lamellipodia protrusion by activating the WAVE2 regulatory complex. *Mol Cell*. 41:661-671.

Myers, M.P., I. Pass, I.H. Batty, J. Van der Kaay, J.P. Stolarov, B.A. Hemmings, M.H. Wigler, C.P. Downes, and N.K. Tonks. 1998. The lipid phosphatase activity of PTEN is critical for its tumor supressor function. *Proc Natl Acad Sci U S A*. 95:13513-13518.

Nakagawa, M., M. Fukata, M. Yamaga, N. Itoh, and K. Kaibuchi. 2001. Recruitment and activation of Rac1 by the formation of E-cadherin-mediated cell-cell adhesion sites. *J Cell Sci*. 114:1829-1838.

Oikawa, T., H. Yamaguchi, T. Itoh, M. Kato, T. Ijuin, D. Yamazaki, S. Suetsugu, and T. Takenawa. 2004. PtdIns(3,4,5)P3 binding is necessary for WAVE2-induced formation of lamellipodia. *Nat Cell Biol*. 6:420-426.

Oldham, S., H. Stocker, M. Laffargue, F. Wittwer, M. Wymann, and E. Hafen. 2002. The *Drosophila* insulin/IGF receptor controls growth and size by modulating PtdInsP(3) levels. *Development*. 129:4103-4109.

Patel, F.B., Y.Y. Bernadskaya, E. Chen, A. Jobanputra, Z. Pooladi, K.L. Freeman, C. Gally, W.A. Mohler, and M.C. Soto. 2008. The WAVE/SCAR complex promotes polarized cell movements and actin enrichment in epithelia during C. elegans embryogenesis. *Dev Biol*. 324:297-309.

Perez, T.D., M. Tamada, M.P. Sheetz, and W.J. Nelson. 2008. Immediate-early signaling induced by E-cadherin engagement and adhesion. *J Biol Chem*. 283:5014-5022.

Pickering, K., J. Alves-Silva, D. Goberdhan, and T.H. Millard. 2013. Par3/Bazooka and phosphoinositides regulate actin protrusion formation during *Drosophila* dorsal closure and wound healing. *Development*. 140:800-809.

Pinal, N., D.C. Goberdhan, L. Collinson, Y. Fujita, I.M. Cox, C. Wilson, and F. Pichaud. 2006. Regulated and polarized PtdIns(3,4,5)P3 accumulation is essential for apical membrane morphogenesis in photoreceptor epithelial cells. *Curr Biol*. 16:140-149.

Qi, Y., J. Liu, J. Chao, P.A. Greer, and S. Li. 2020. PTEN dephosphorylates Abi1 to promote epithelial morphogenesis. *J Cell Biol*. 219.

Rauzi, M., and P.F. Lenne. 2015. Probing cell mechanics with subcellular laser dissection of actomyosin networks in the early developing *Drosophila* embryo. *Methods Mol Biol*. 1189:209-218.

Ridley, A.J., H.F. Paterson, C.L. Johnston, D. Diekmann, and A. Hall. 1992. The small GTP-binding protein rac regulates growth factor-induced membrane ruffling. *Cell*. 70:401-410.

Rottner, K., T.E.B. Stradal, and B. Chen. 2021. WAVE regulatory complex. *Curr Biol*. 31:R512-R517.

Schaks, M., S.P. Singh, F. Kage, P. Thomason, T. Klunemann, A. Steffen, W. Blankenfeldt, T.E. Stradal, R.H. Insall, and K. Rottner. 2018. Distinct Interaction Sites of Rac GTPase with WAVE Regulatory Complex Have Non-redundant Functions in Vivo. *Curr Biol*. 28:3674-3684 e3676.

Seppa, M.J., R.I. Johnson, S. Bao, and R.L. Cagan. 2008. Polychaetoid controls patterning by modulating adhesion in the *Drosophila* pupal retina. *Dev Biol*. 318:1-16.

Stowers, R.S., and T.L. Schwarz. 1999. A genetic method for generating *Drosophila* eyes composed exclusively of mitotic clones of a single genotype. *Genetics*. 152:1631-1639.

Suetsugu, S., S. Kurisu, T. Oikawa, D. Yamazaki, A. Oda, and T. Takenawa. 2006. Optimization of WAVE2 complex-induced actin polymerization by membrane-bound IRSp53, PIP(3), and Rac. *J Cell Biol*. 173:571-585.

Traynor-Kaplan, A.E., A.L. Harris, B.L. Thompson, P. Taylor, and L.A. Sklar. 1988. An inositol tetrakisphosphate-containing phospholipid in activated neutrophils. *Nature*. 334:353-356.

Trivedi, D., V. Cm, K. Bisht, V. Janardan, A. Pandit, B. Basak, S. H, N. Ramesh, and P. Raghu. 2020. A genome engineering resource to uncover principles of cellular organization and tissue architecture by lipid signaling. *Elife*. 9.

von Stein, W., A. Ramrath, A. Grimm, M. Muller-Borg, and A. Wodarz. 2005. Direct association of Bazooka/PAR-3 with the lipid phosphatase PTEN reveals a link between the PAR/aPKC complex and phosphoinositide signaling. *Development*. 132:1675-1686.

Weinkove, D., S.J. Leevers, L.K. MacDougall, and M.D. Waterfield. 1997. p60 is an adaptor for the *Drosophila* phosphoinositide 3-kinase, Dp110. *J Biol Chem*. 272:14606-14610.

Wernet, M.F., T. Labhart, F. Baumann, E.O. Mazzoni, F. Pichaud, and C. Desplan. 2003. Homothorax switches function of *Drosophila* photoreceptors from color to polarized light sensors. *Cell*. 115:267-279.

Whitman, M., C.P. Downes, M. Keeler, T. Keller, and L. Cantley. 1988. Type I phosphatidylinositol kinase makes a novel inositol phospholipid, phosphatidylinositol-3-phosphate. *Nature*. 332:644-646.

Yamada, S., and W.J. Nelson. 2007. Localized zones of Rho and Rac activities drive initiation and expansion of epithelial cell-cell adhesion. *J Cell Biol*. 178:517-527.

Zallen, J.A., Y. Cohen, A.M. Hudson, L. Cooley, E. Wieschaus, and E.D. Schejter. 2002. SCAR is a primary regulator of Arp2/3-dependent morphological events in *Drosophila*. *J Cell Biol*. 156:689-701.

FIGURE LEGENDS

Figure 1: *pten* affects epithelial junctional remodeling and ommatidia structure

(A) Left: Schematics of major steps in lattice remodeling. Right: Types of LCs, periods of expansion and contraction of LC–LC contacts and contracted or expanded contacts in this and subsequent figures. (B-C) Ommatidia in adult eyes that are (B, B') WT or (C, C') *pten* mutant. (D-G) Cellular defects in *pten* mutant eyes with different alleles compared with WT, 36-40h APF. (D) WT; each bristle cell, and 3° LC, connects to three 2° LCs. (E) $pten^{2L100}$ mutant; common defects include cellular rosettes and LC-LC contacts lost and replaced by 1°-1° contacts (F-G) $pten^{3}$ and $pten^{c494}$ mutants; defects are similar to $pten^{2L100}$ but more severe. (H-K) Quantification of counts of specific defect types in the *pten* mutants compared with WT. *pten* mutant eyes exhibit more (H) ommatidia that are not six-sided, (I) vertices with multiple bristles, (J) cellular rosettes and (K) edges missing LCs and/or exhibiting aberrant 1°-1° contacts. χ^2 tests; ****$p < 0.0001$. (L) A negatively marked *pten* mutant clone generated using the FLP/FRT system (outlined in yellow). Yellow arrowheads mark cellular rosettes; purple arrowheads mark aberrant 1°-1° contacts. (M-N) Quantifications of the mutant and WT cell composition of (M) rosettes and (N) aberrant edges in eyes containing $pten^{2L100}$ and $pten^{3}$ mutant clones compared with WT.

Figure 2: *pten* affects contact pulsing during eye epithelial remodeling

(A) Cellular dynamics in a WT ommatidium during pruning and shape changes of LCs, 26-28 AFP. Detail is of a row of LCs and a kymograph of a single contact at 2-minute intervals. When a cell prunes from the lattice, a new contact is immediately established between the cells on either side. LC-LC contacts expand and contract repeatedly over periods of 10-20 minutes. (B) Dynamics of cells in a *pten* ommatidium. Above: Snapshots of an LC being pruned from the lattice. After the cell delaminates, adjacent cells remain separated, creating a contact between two 1° cells (white arrowheads) that is repaired over the next hour. Below: Snapshots and kymograph of a pulsing LC-LC contact. Compared with WT, expansions and contractions are small and uncoordinated, and the contact remains short overall. (C-F) Quantifications of contact length pulses in WT and *pten* mutant eyes. (C) Mean contact length (D) Pulse amplitude (E) Pulse amplitude

normalized to mean contact length (F) Pulse frequency. Statistics were performed using the Mann-Whitney *u* test, n=20 WT, 30 *pten* contacts from 2-3 eyes. *p>.05, ****p>.0001.

Figure 3: *pten* affects contractile and protrusive dynamics during contact pulsing

(A-D) Dynamics of (A-B) F-actin and (C-D) MyoII in (A, C) WT and (B, D) *pten* mutants, 26-28h APF. (E-H) Time-shifted Pearson's correlations between contact length and levels of (E-F) F-actin and (G-H) MyoII in the above two genotypes. In this and subsequent graphs, the black line represents the mean R-value and gray bars indicate the SD. For each graph, n=30 contacts were pooled from 3 eyes. (E) Length vs. F-actin, WT. Peak mean R-value is .52 at a shift of -2. (F) Length vs F-actin, *pten*. Peak mean R-value is .13 at a shift of -7. (G) Length vs. MyoII, WT. Peak mean R-value is -.48 at a shift of -1. (H) Length vs MyoII, *pten*. Peak mean R-value is -.14 at a shift of-2. (I-J) Comparisons of correlations between length and (I) F-actin or (J) MyoII for individual WT and *pten* contacts at time-shift of WT peak mean R-value. n=30 contacts per genotype pooled from 3 eyes. (K-L) Comparison of mean pulse amplitudes of (K) F-actin and (L) MyoII normalized to mean reporter levels over 60 minutes at vertices of individual contacts. Statistics: Mann-Whitney *u* test, ***p<.001, ****p<.0001.

Figure 4: *pten* affects Abi dynamics during eye epithelial remodeling

(A-B) Dynamics of Abi in (A) WT eyes and (B) fully mutant *pten* eyes. (C) Comparison of pulse amplitude of Abi at vertices normalized to mean Abi. N=30 WT, 30 *pten* contacts pooled from 3-4 eyes per genotype. Unpaired t-test with Welch's correction, p>.0001. (D) Comparison of Abi pulse frequency. Mann-Whitney *u* test, p=.0209. (E-F) Time-shifted Pearson's correlations between contact length and Abi levels in WT and *pten* eyes. (E) WT. Peak mean R-value is .39 at a shift of -3. (F) *pten*. Peak mean R-value is .21 at a shift of -3. (G) Comparison of R-values at a -3 timeshift in both genotypes. Unpaired t-test, p>.0001. (H-I) Snapshots and kymographs of laser ablations of LC-LC contacts in (H) a WT eye and (I) a *pten* mutant eye. Yellow stars mark sites of ablation. (J-K) Recoil curves of 10 ablations each from (J) a single WT eye and (K) a single *pten* eye. (L) The initial recoil velocity (V_{max}) of individual contacts pooled across 3 eyes in WT compared with

pten mutants. Unpaired t-test, n=18-25 contacts.

Figure 5: *pten* affects PIP_3 dynamics during eye epithelial remodeling

(A) Levels and localization of PIP_3 in FLP/FRT generated *pten* mutant clones, 28-30h APF. (B-C) Dynamics of PIP_3 in (B) WT eyes and (C) eyes fully mutant for *pten*. (D) Comparison of pulse amplitude of PIP_3 normalized to mean PIP_3. N=20 WT, 29 *pten* contacts pooled from 2-3 eyes per genotype. Unpaired t-test with Welch's correction, p<.0001. (E) Comparison of PIP_3 pulse frequency. Unpaired t-test, p=.04975. (F-G) Time-shifted Pearson's correlations between contact length and PIP_3 levels in WT and *pten* eyes. (F) WT. Peak mean R-value is .54 at a shift of -3. (G) *pten*. Peak mean R-value is .02 at a shift of +13. (H) Comparisons of R-values at a shift of -3 versus a shift of 0 in WT. Paired t-test, p=.0002 (I) Comparison of R-values at a shift of -3 in both genotypes. Unpaired t-test, p=.0002.

Figure 6: Pi3K Loss- and gain-of-function disrupt eye epithelial remodeling

(A) PIP_3 pulsing in clones expressing Pi3K-cat.CAAX (B) Pulse amplitudes of PIP_3 normalized to total PIP_3 in clones compared with WT regions. Mann-Whitney *u* test, p<.0001, n=16-22 contacts pooled from 4 eyes. (B') Time-shifted Pearson's correlations between length and PIP_3 in clone regions expressing Pi3K-cat.CAAX (peak correlation .17 at -5). (C) LC-LC contact dynamics in an eye fully mutant for Pi3K-reg. (D) Quantification of (D) absolute and (D') normalized pulse amplitudes in *Pi3K-reg* mutant eyes compared to WT. Mann-Whitney *u*-test, n=20 contacts ****p<.0001. (E-F) Dynamics of (E) F-actin and MyoII and (F) the WRC in *Pi3K-reg* mutant eyes. (E', F') Time-shifted Pearson's correlations between contact length and (H') the WRC (peak correlation -.11 at shift of +2), (F') F-actin (peak correlation .15 at a shift of +4), and (F'') MyoII (peak correlation .30 at a shift of -3).

Figure 7: *pten* affects Rac signaling, which in turn affects the WRC and protrusive F-actin dynamics

(A-B) Dynamics of GFP-tagged Rac1 in (A) a WT eye and (B) a *pten* mutant eye. (C-D) Comparisons of pulse (C) amplitudes and (D) frequencies of Rac1 at contact vertices in the two genotypes. (T-test, n=28 WT, 20 *pten*, *p<.05,

***p<.001). (E-F) Time-shifted Pearson's correlations between contact length and Rac1 intensity in WT and *pten*. (E) WT: peak R-value = .21 at shift of 0, significantly different from R-value of 0, one-sample t-test, p<.05, n=28 contacts from 3 eyes (F) *pten*: peak R-value =.16 at a shift of +1, no significant difference from R-value of 0, one sample t-test, p=.1493, n=20 contacts from 2 eyes. (G) Comparison between R-values at 0 for both genotypes, unpaired t-test, p=.6800. (H-J) Dynamics of (H) PIP_3 (I) the WRC and (J) F-actin in eyes expressing Rac1. Ordinary patterns of accumulation along with contact expansion/contraction are abolished. (K-M) Quantifications of localization of (K) PIP_3, (L) the WRC and (M) F-actin in eyes overexpressing Rac1. All three molecules are more concentrated at vertices in Rac1 overexpression compared to control. Unpaired t-tests, **p<.01, ****p<.0001. n=29-66 contacts pooled from 2-4 eyes per genotype.

Figure 8: Pi3K-reg accumulates preferentially and dynamically along LC-LC contacts

(A) Dynamics of GFP-tagged Pi3K-reg and F-actin in a WT eye. Pi3K localizes to the vertex in expanded contacts, while in contracted contacts, it localizes primarily in spots around the vertex. (B) Time-shifted Pearson's correlations between contact length and Pi3K (B) directly at the vertex (peak mean R-value .54 at a shift of 0) and (B') adjacent to the vertex, (peak mean R-value .34 at a shift of -3). (C) Time-shifted Pearson's correlations between F-actin and Pi3K (C) at the vertex (peak mean R-value=.58 at a time shift of +1) and (C') adjacent to the vertex (peak mean R-value=.55 at a shift of 0). N=30 contacts pooled from 3 eyes for each correlation. (D) Two rows of cells expressing Pi3K-reg::GFP and stained for Sdk and E-cad. White arrowheads: sites of colocalization between Pi3K and E-cad. Orange arrowheads: sites of colocalization between Pi3K and Sdk. (E) Dynamics of GFP-tagged Pten and F-actin in a WT eye. (F-G) Time-shifted Pearson's correlations of Pten levels with (F) contact length and (G) F-actin. Pten does not show a strong correlation with contact length (peak R-value .10 at shift of -9) but does correlate with F-actin (peak R-value .67 at shift of 0).

Figure 9: Graphical summary of the control of contact length pulsing by Pi3K, Pten and PIP_3. Pi3K regulates the transition from contraction to expansion through its tension-dependent localization to tAJs and modulation of its lipid phosphatase activity. Pten localizes uniformly to regulate PIP_3 turnover and attenuate PIP_3 production. (A) Tension

shortens contacts, concentrates Pi3K at four spots at a distance from tAJs, and inhibits Pi3K's lipid phosphatase function. (B) High tension ultimately disassembles contractile networks allowing Pi3K to flow toward tAJs, produce PIP_3 and activate the WRC to promote F-actin branching and contact expansion. (C) High protrusion in expanded contacts disperses the WRC and disassembles the branched F-actin network. (D) Branched F-actin disassembly allows the assembly and contraction of an actomyosin network, which increases tension and contracts the contact leading to the flow of Pi3K away from tAJs and inhibition of its lipid phosphatase function, thus completing the cycle.

SUPPLEMENTARY MATERIALS

Supplemental Figure 1: Pten lipid phosphatase activity is required for epithelial remodeling

(A-D) GFP-marked *pten* clones in a background expressing (A) no transgene, (B) WT Pten, (C) Pten (G137E) deficient for protein and lipid phosphatase activity, and (D) Pten (C132S) deficient for lipid phosphatase activity only. (E) A GFP-marked clone in a WT background expressing WT Pten as a positive control. (F) GFP-marked *pten* clones with RNAi mediated knockdown of Pi3K-cat. (F) Counts of cellular rosettes in clones of the above five genotypes as a proxy for overall lattice disorganization. Expressing WT Pten accomplishes a nearly complete rescue of the *pten* phenotype, while the G137E and C132S variants provide little to no rescue. RNAi depletion of Pi3K accomplishes a partial rescue as well.

Supplemental Figure 2: Effects of Pi3K on lattice remodeling and PIP_3 levels

(A-C) 28h APF clones in three genotypes affecting P_I3K function, all expressing tubulin-GPH. (A) Act>Pi3K-cat.CAAX (B) Act>Pi3K-cat.RNAI (C) *Pi3K-reg* -/-. (D-F) Cellular defects in three genotypes affecting Pi3K function, 34-38h APF. (A) Ey>Pi3K-cat.CAAX (B) Ey>Pi3K-cat.RNAi (C) EGUF eye fully mutant for *Pi3K-reg*. (G-I) Quantification of counts of specific defect types in the above genotypes compared with WT. Both overexpression and knockdown of Pi3K function increase the numbers of (G) edges missing LCs, (H) vertices with multiple bristles, and (I) cellular rosettes. (J) Dynamics of PIP_3 in a clone expressing Act>Pi3K-cat RNAi. In addition to overall levels, PIP_3 pulsing is reduced. (K-L) Clones expressing Ecad::GFP and (K, K') Act>Pi3K-cat.CAAX or (L, L') Act>Pi3K-cat.RNAi, displaying (K, L) cellular defects and (K', L') reduced pulsing between LC-LC contacts. Quantification of (M-N) absolute and (M'-N') normalized pulse amplitudes in clones expressing (M) Pi3K-cat.CAAX and (N) Pi3K-cat.RNAi compared to adjacent WT regions. Unpaired t-test, n=9-18 contacts *p<.05.

Supplemental Figure 3: Large-scale tissue disruptions in Rac1-overexpressing eyes

(A) Snapshots of an expanding tissue rupture. Expansions of the rupture are accompanied by F-actin bursts, while MyoII extends into the hole formed by the rupture. (B) Snapshots of another rupture, this time with tagged WRC and F-actin,

which are both enriched at its edges as it expands. (C) Snapshots of a rupture with labeled PIP_3 enriched at breaking contacts. (D) GFP-marked clones overexpressing Rac1. Arrowheads mark ruptured cells. (E) GFP-marked clones overexpressing Rac1 in a *SCAR* -/- background. An arrowhead marks a ruptured cell, of which there are overall fewer. (F) GFP-marked clones overexpressing Rac1 in a *pten* -/- background. There are no ruptured cells and few surviving mutant LCs, though non-autonomous defects persist in surrounding ommatidia.

Supplemental movie 1: Cellular dynamics in WT compared with *pten* mutant eyes. (Corresponds to Fig. 2)
Left: Time-lapse of a WT eye showing normal dynamics of repeated cell contact expansion and contraction during lattice remodeling (white arrowhead). When the cell prunes from the lattice, contact between neighboring cells is reestablished immediately (yellow arrowhead). Right: A *pten* mutant eye with a disordered ommatidium demonstrating pinched contacts that fail to expand and contract (white arrowhead) and separations between LCs following cell pruning that take 10-30 minutes to repair (yellow arrowhead).

Supplemental movie 2: F-actin dynamics in WT compared with *pten* mutant eyes. (Corresponds to Fig. 3)
Left: Time-lapse of a WT eye showing dynamics of F-actin. Note accumulation of F-actin while contact is expanding and disassembly during contraction. Right: Time-lapse of a *pten* eye showing dynamics of F-actin.

Supplemental movie 3: Myosin dynamics in WT compared with *pten* mutant eyes (Corresponds to Fig. 3)
Left: Time-lapse of a WT eye showing dynamics of MyoII. Note accumulation of MyoII in contracting contact and lower MyoII levels in expanded contact. Right: Time-lapse of a *pten* eye showing dynamics of MyoII. MyoII appears in more clearly defined cables than in WT but does not accumulate and dissipate along with contact expansion and contraction, respectively.

Supplemental movie 4: WRC dynamics in WT compared with *pten* mutant eyes (Corresponds to Fig. 4)

Left: Time-lapse of a WT eye showing dynamics of the WRC. Note accumulation while the contact is expanding and dispersal during contraction. Right: Time-lapse of a *pten* eye showing dynamics of the WRC.

Supplemental movie 5: Laser ablation of contacts in WT and *pten* mutant eyes (Corresponds to Fig. 4)

Left: Laser ablation of an LC-LC contact in a WT eye. Right: Laser ablation of an LC-LC contact in a *pten* mutant eye.

Supplemental movie 6: PIP_3 dynamics in WT compared with *pten* mutant eyes (Corresponds to Fig. 5)

Left: Time lapse of a WT eye showing dynamics of PIP_3 with E-cad (Shg) for cell outlines. Note accumulation while the contact is expanding and dispersal during contraction. Center: The same ommatidium with only PIP_3. Right: Time-lapse of a *pten* eye showing PIP_3 dynamics.

Supplemental movie 7: PIP_3 dynamics in clones with increased or reduced Pi3K-cat activity. (Corresponds to Fig. 6)

Left: Time lapse of PIP_3 dynamics in a clone expressing Pi3K-cat.CAAX (marked in red) and adjacent WT region. Right: Time lapse of PIP_3 dynamics in a clone expressing Pi3K-cat RNAi (marked in red) and adjacent WT region. Details show close-ups of rows of clone cells.

Supplemental movie 8: Dynamics of cells and force generators in *Pi3K-reg* mutant eyes (Corresponds to Fig. 6)

Left: An ommatidium from a *Pi3K-reg* mutant eye in which LC-LC contacts fail to expand and contract. Center: Time lapse of F-actin dynamics in a *Pi3K-reg* mutant eye. Right: Time lapse of WRC dynamics in a *Pi3K-reg* mutant eye.

Supplemental movie 9: Rac dynamics in WT compared with *pten* mutant eyes (Corresponds to Fig. 7)

Left: Time-lapse of a WT eye showing dynamics of Rac1. Note accumulation while contact is expanding and dispersal during contraction. Right: Time-lapse of a *pten* eye showing dynamics of Rac1.

Supplemental movie 10: Abnormal dynamics of F-actin, the WRC, and PIP_3 in eyes overexpressing Rac1 (Corresponds to Fig. 7) Dynamics of F-actin (Left) the WRC (Center) and PIP_3 (Right) in eyes overexpressing Rac1. Fluctuations of contact length are reduced, and all three molecules remain overly concentrated at contact vertices.

Supplemental movie 11: Tissue ruptures in eyes overexpressing Rac1 (Corresponds to Fig. 7)

Top: Tissue rupture expanding in an eye expressing tagged F-actin and MyoII. Middle: Tissue rupture forming and expanding in an eye expressing tagged Abi and F-actin. Bottom: Tissue rupture forming in an eye expressing tagged GRP1-PH to label PIP_3.

Supplemental movie 12: Dynamics of Pi3K-reg and Pten (Corresponds to Fig. 8)

Left: An ommatidium in an eye expressing tagged Lifeact and Pi3K-reg. Note accumulation of Pi3K at vertices in expanded contacts and in dimmer spots adjacent to vertices in contracted contacts. Right: An ommatidium in an eye expressing tagged Lifeact and Pten2.

Figure 1

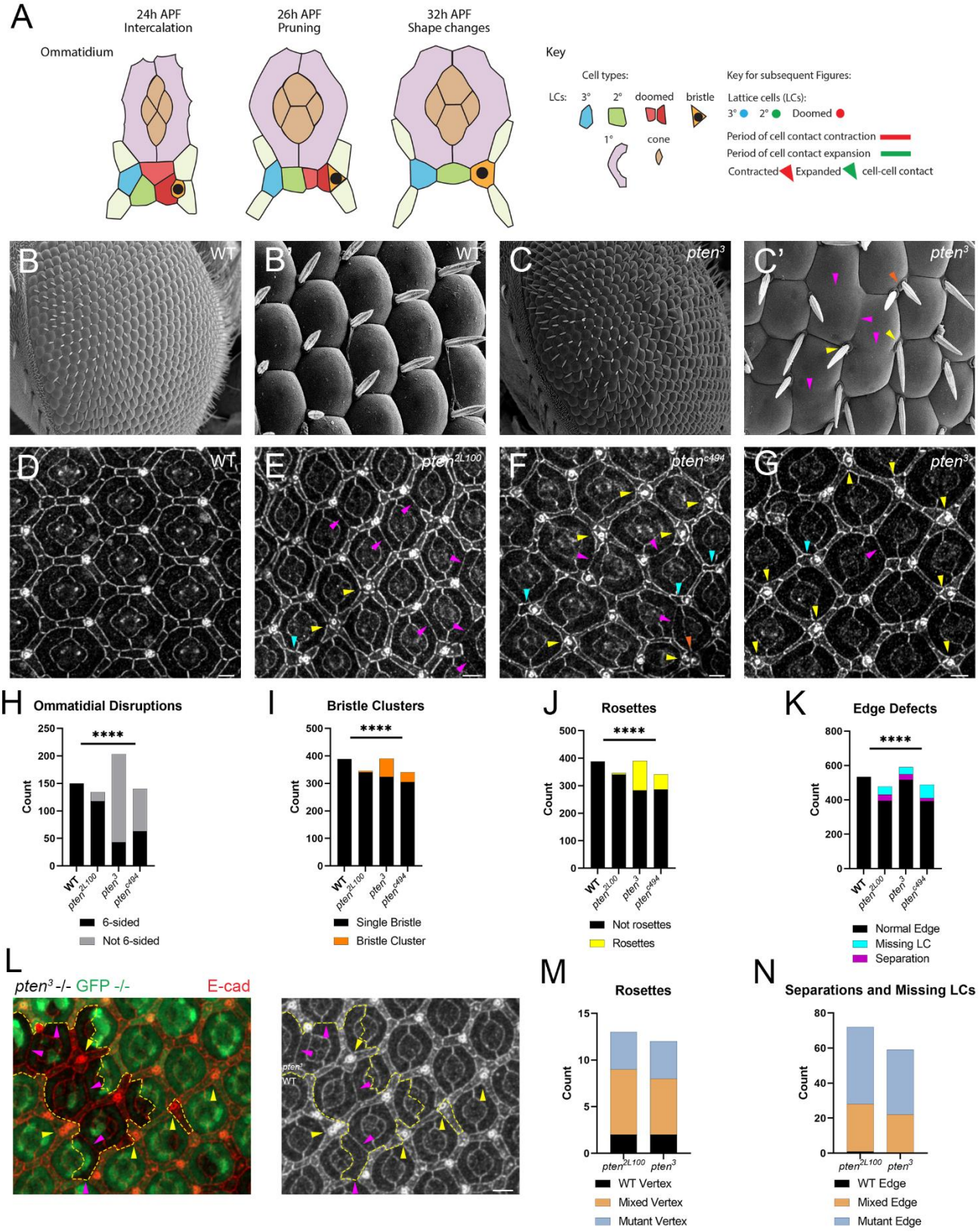

Figure 2

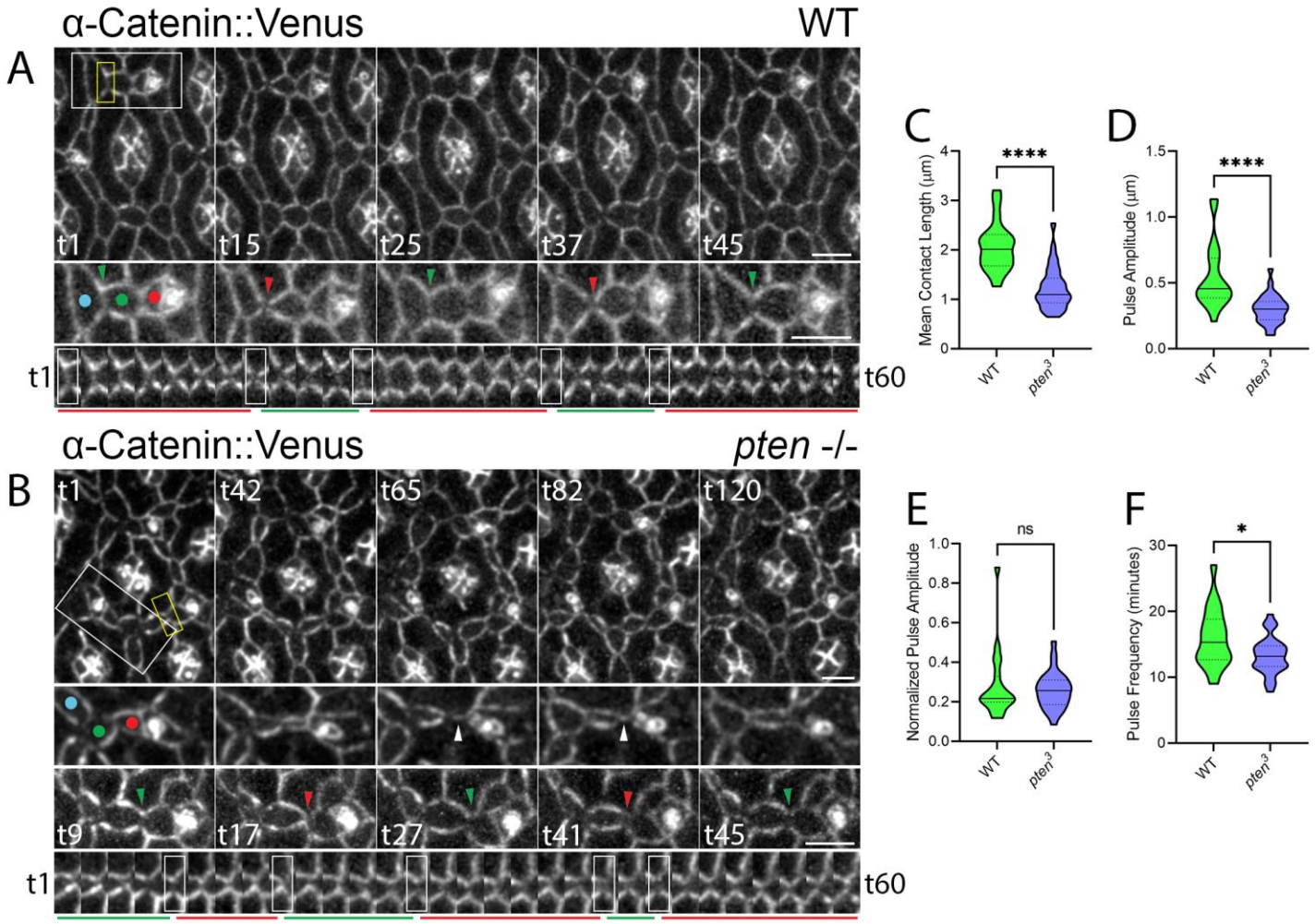

Figure 3

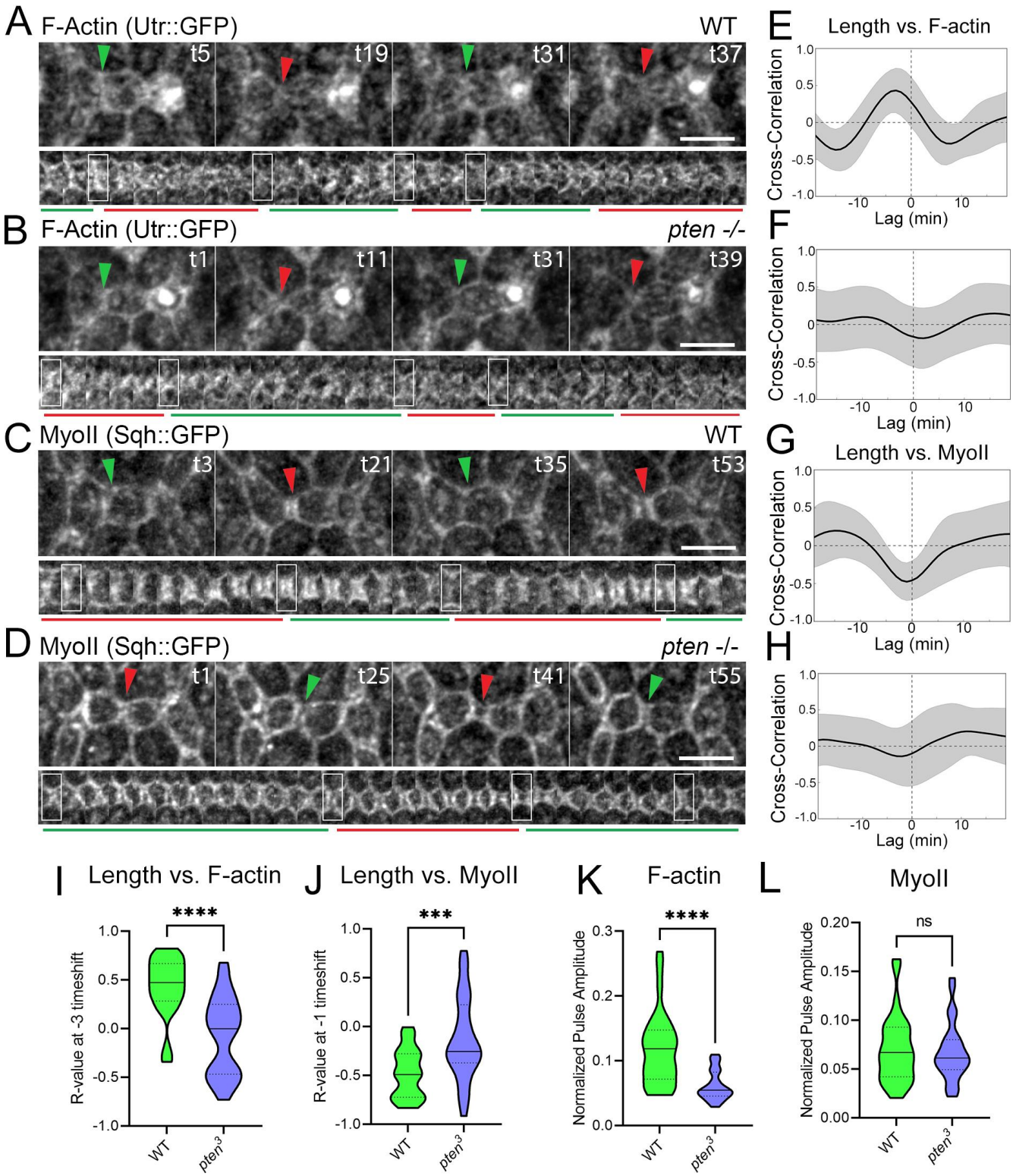

Figure 4

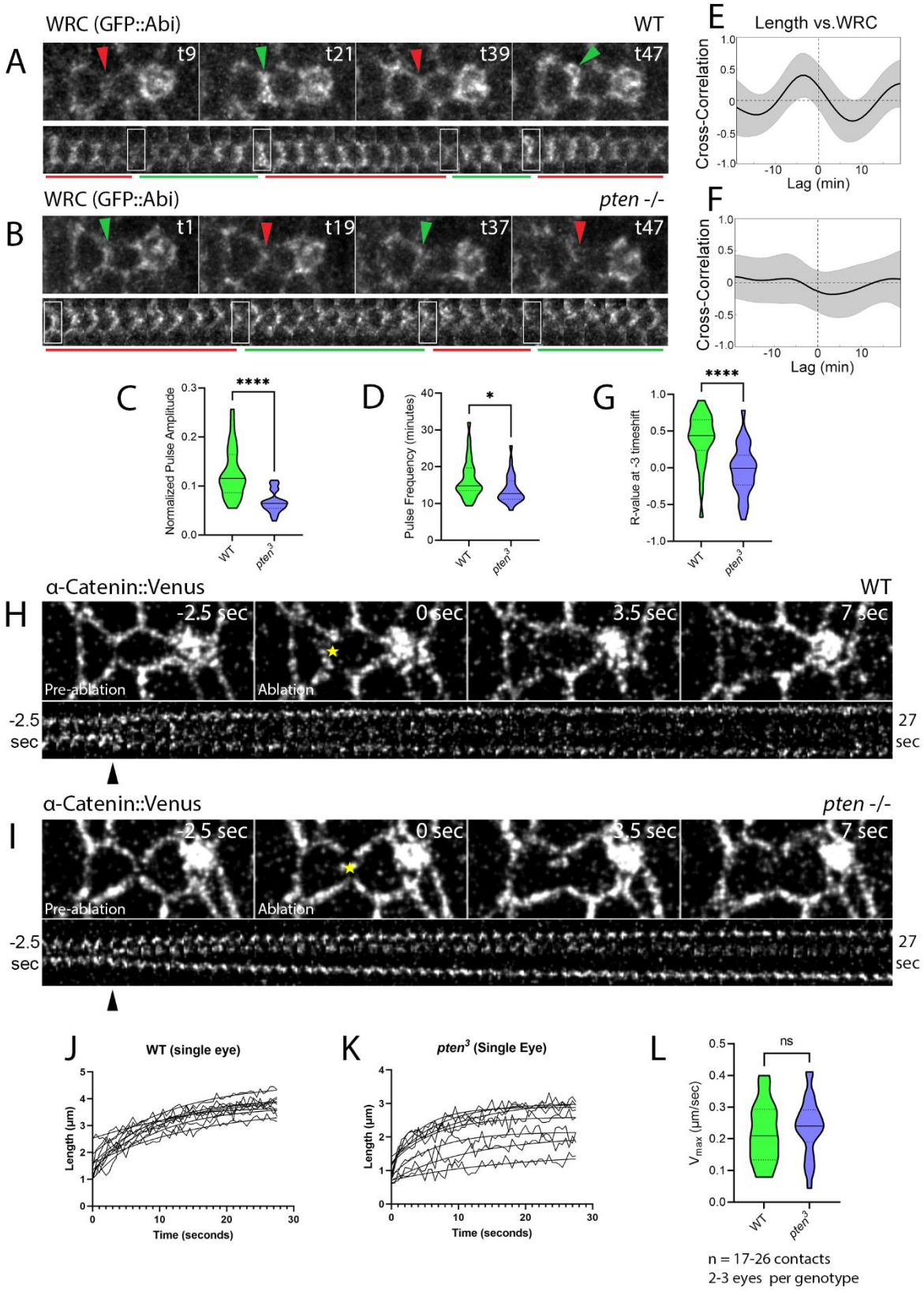

Figure 5

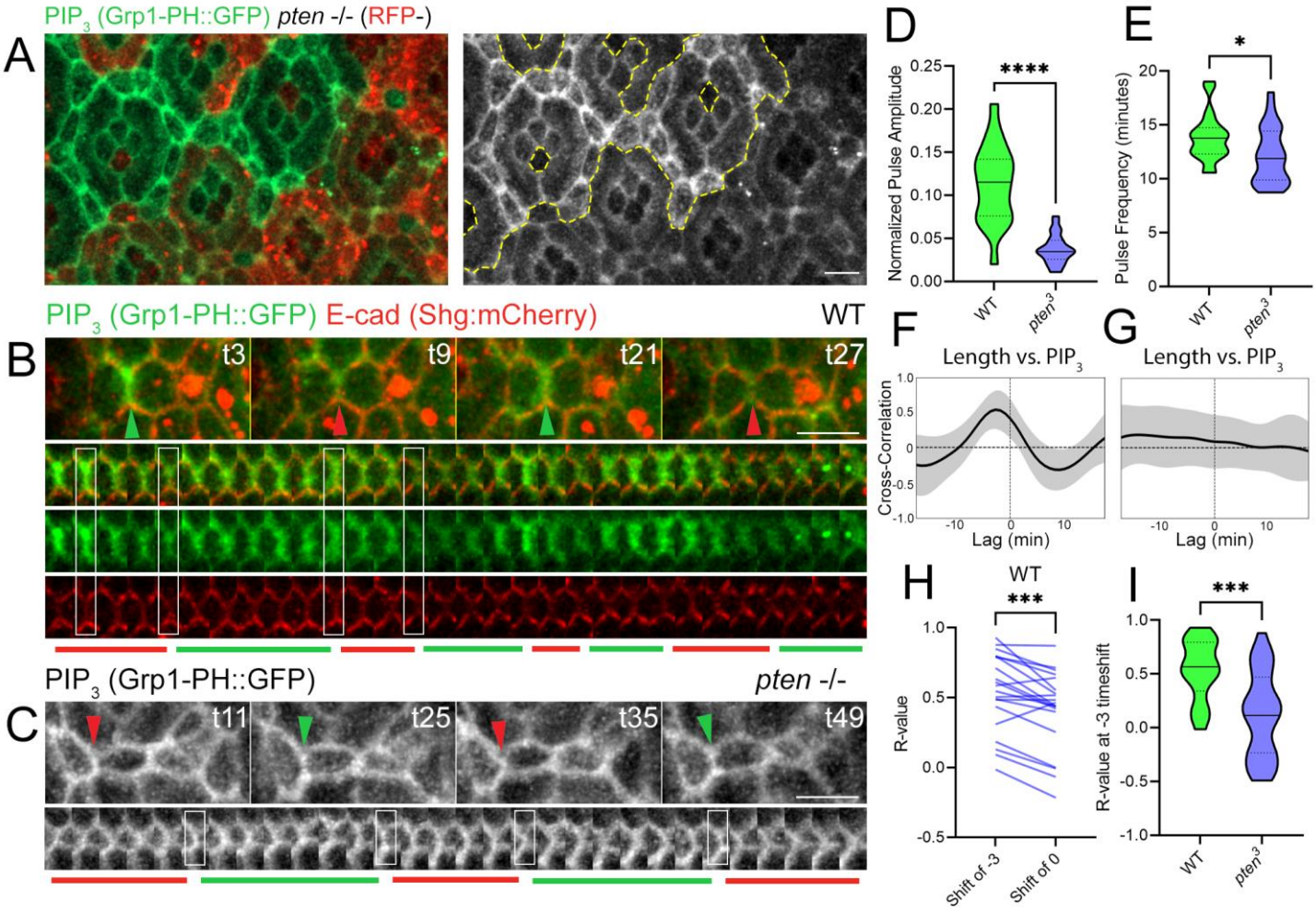

Figure 6

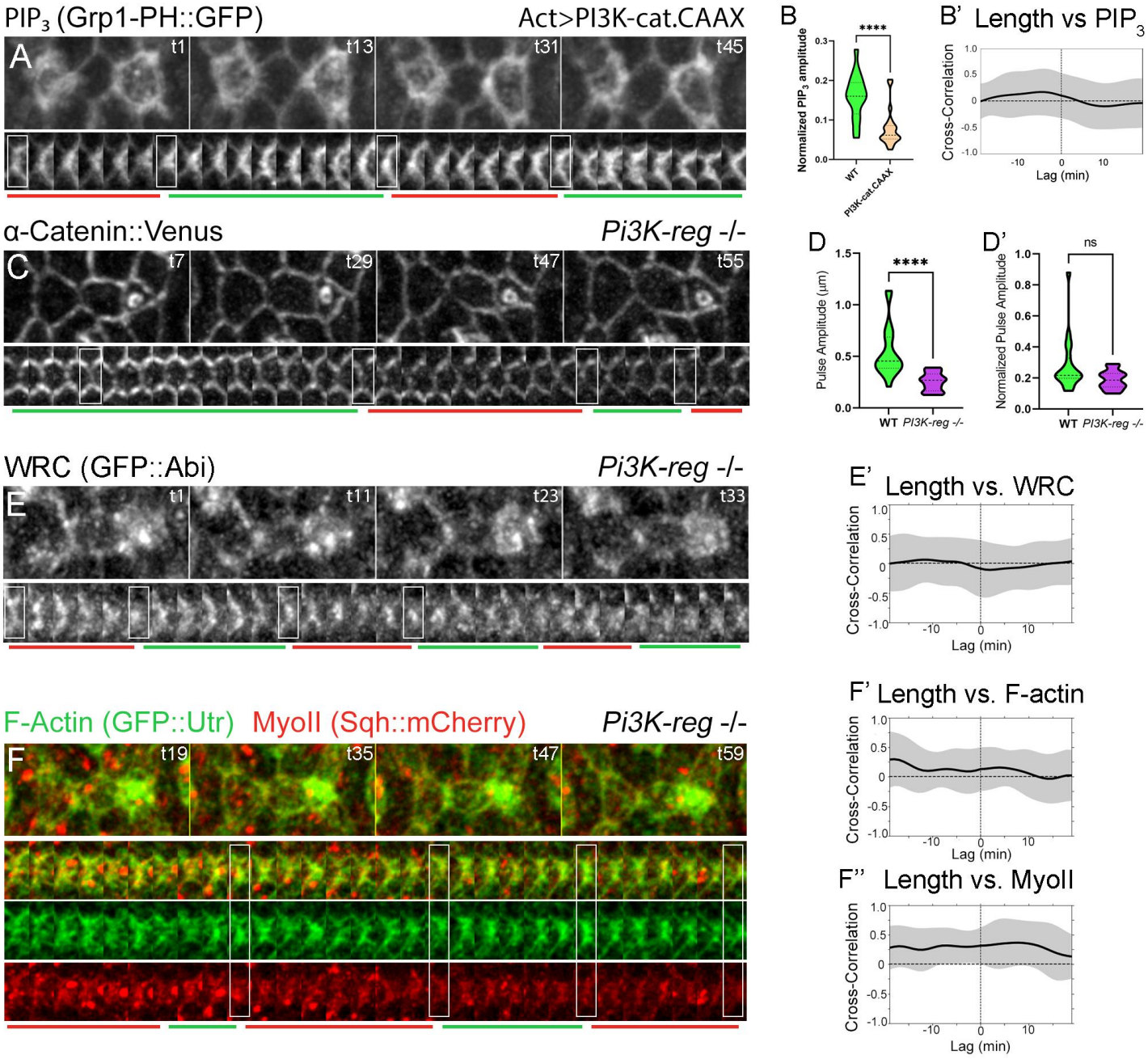

Figure 7

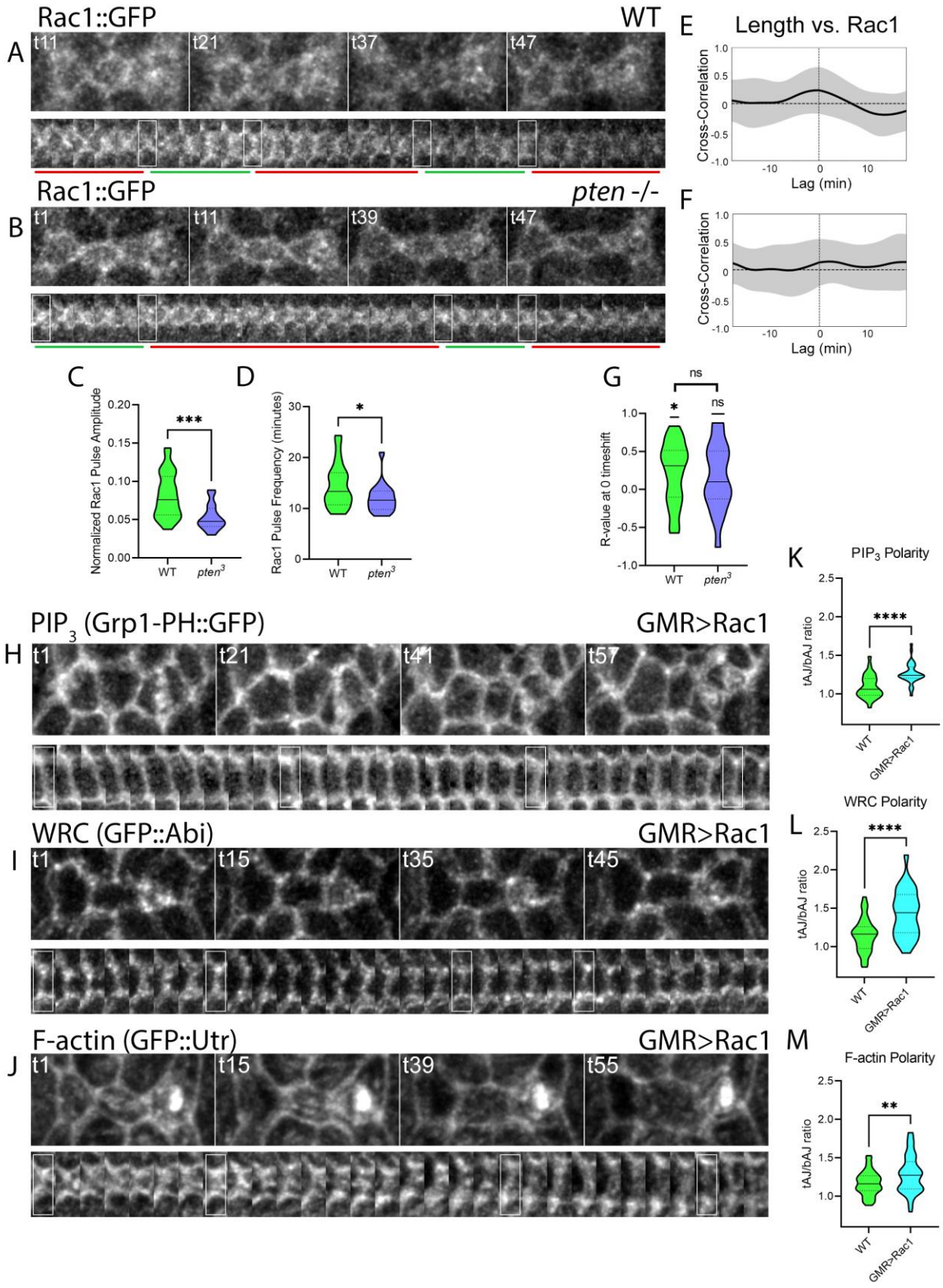

Figure 8

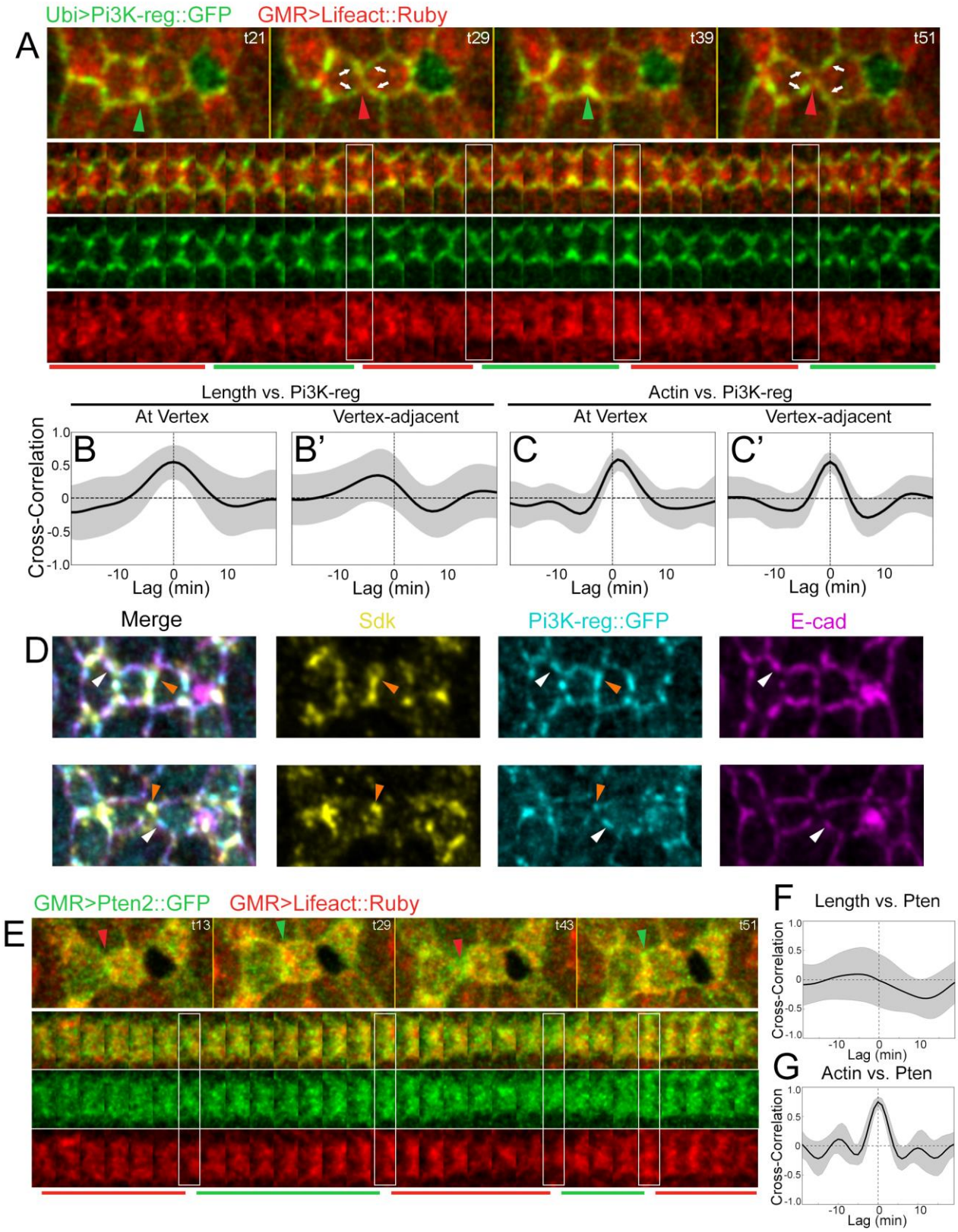

Figure 9

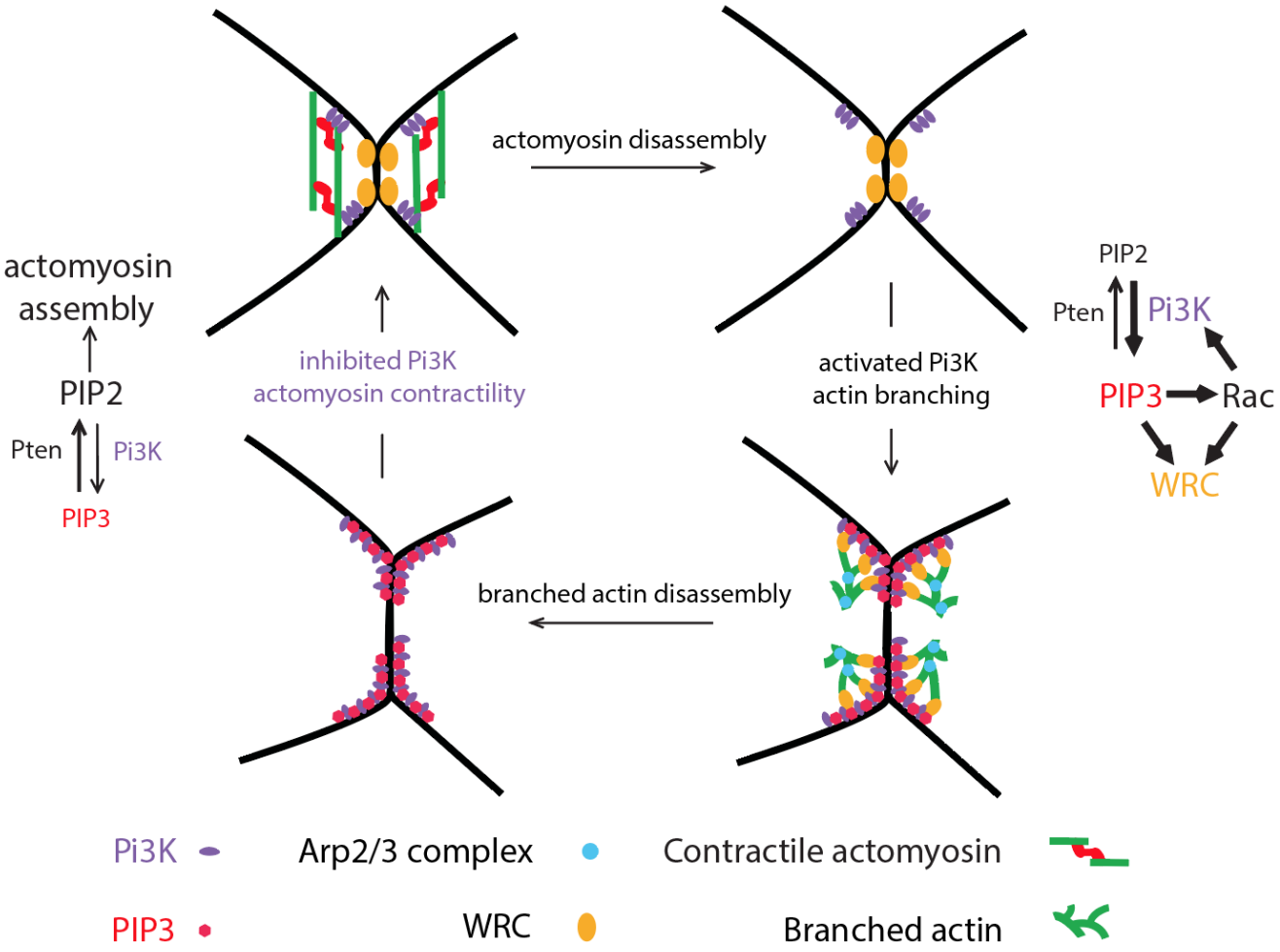

Figure S1

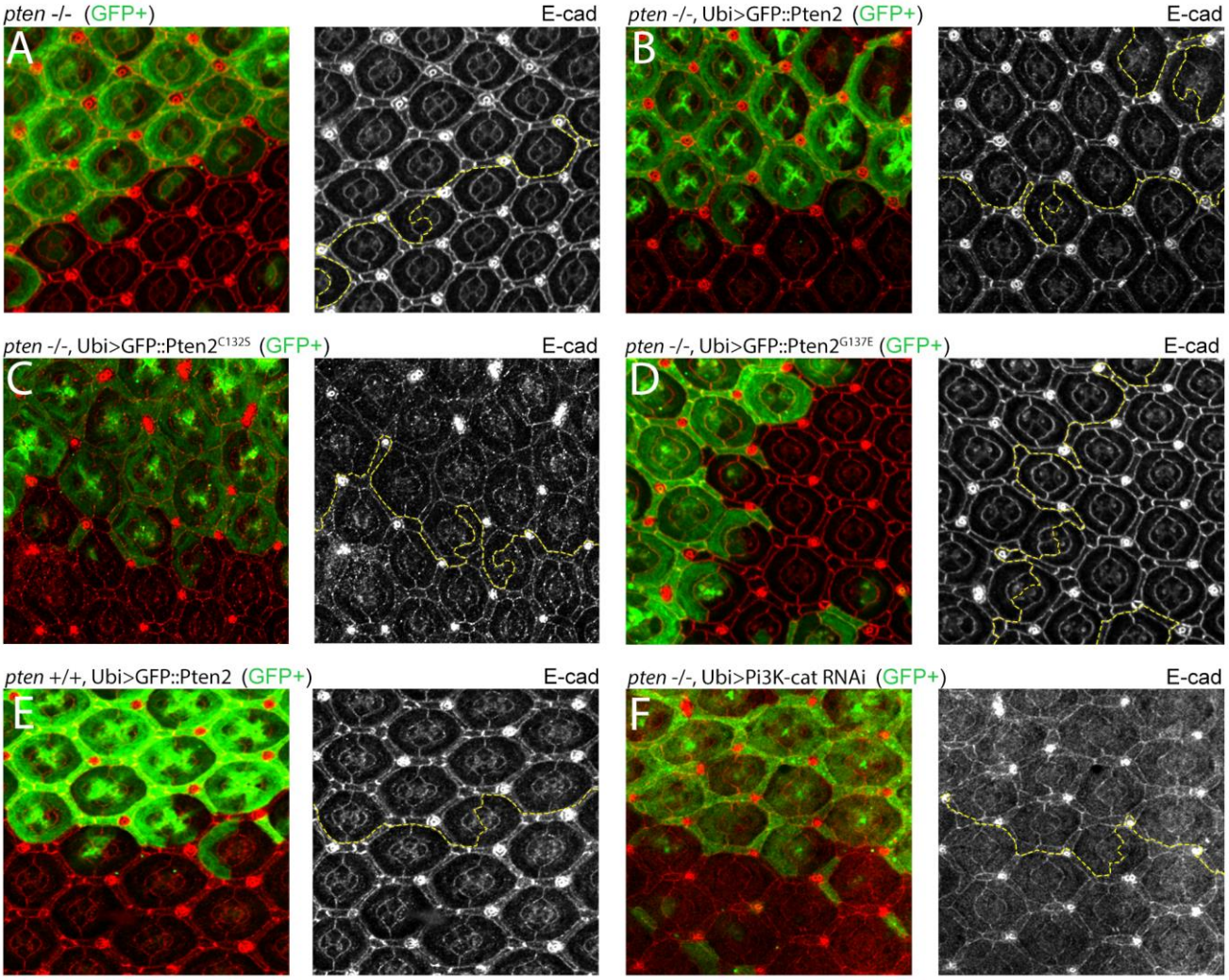

Figure S2

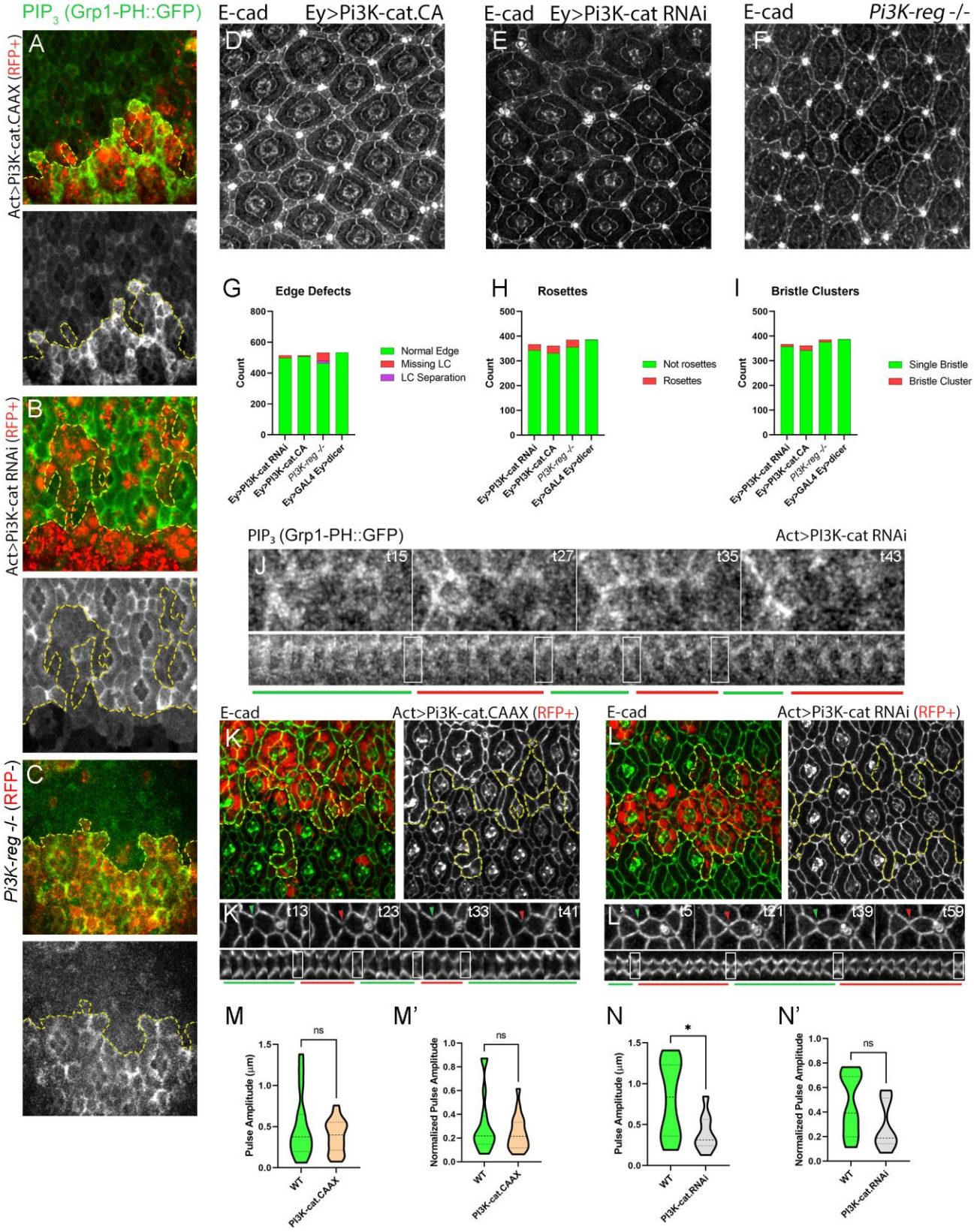

Figure S3